HHS Public Access

Author manuscript

Cancer Discov. Author manuscript; available in PMC 2020 May 01.

Published in final edited form as:

Cancer Discov. 2019 November ; 9(11): 1606–1627. doi:10.1158/2159-8290.CD-18-1261.

The AMPK-related kinases SIK1 and SIK3 mediate key tumor suppressive effects of LKB1 in NSCLC.

Pablo E. Hollstein[1], **Lillian J. Eichner**[1], **Sonja N. Brun**[1], **Anwesh Kamireddy**[1], **Robert U. Svensson**[1], **Liliana I. Vera**[1], **Debbie S. Ross**[1], **T.J. Rymoff**[1], **Amanda Hutchins**[1], **Hector M. Galvez**[1], **April E. Williams**[2], **Maxim N. Shokhirev**[2], **Robert A. Screaton**[3], **Rebecca Berdeaux**[4], **Reuben J. Shaw**[1,*]

[1]Molecular and Cell Biology Laboratory, The Salk Institute for Biological Studies, 10100 N Torrey Pines Road, La Jolla, CA, USA

[2]Razavi Newman Integrative Genomics and Bioinformatics Core, The Salk Institute for Biological Studies, 10100 N Torrey Pines Road, La Jolla, CA, USA

[3]Sunnybrook Research Institute, and Department of Biochemistry, University of Toronto, Toronto, Ontario, Canada

[4]Department of Integrative Biology and Pharmacology, McGovern Medical School at the University of Texas Health Science Center at Houston, Houston, Texas, USA

Abstract

Mutations in the LKB1 (*STK11*) tumor suppressor are the third most frequent genetic alteration in non-small-cell lung cancer (NSCLC). LKB1 encodes a serine/threonine kinase that directly phosphorylates and activates 14 AMPK family kinases ("AMPKRs"). The function of many of the AMPKRs remains obscure, and which are most critical to the tumor suppressive function of LKB1 remains unknown. Here we combine CRISPR and genetic analysis of the AMPKR family in NSCLC cell lines and mouse models, revealing a surprising critical role for the SIK subfamily. Conditional genetic loss of *Sik1* revealed increased tumor growth in mouse models of *Kras*-dependent lung cancer, which was further enhanced by loss of the related kinase *Sik3*. As most known substrates of the SIKs control transcription, gene expression analysis was performed, revealing upregulation of AP-1 and IL6 signaling in common between LKB1- and SIK1/3-

*Correspondence: Reuben J. Shaw, Molecular and Cell Biology Laboratory, The Salk Institute for Biological Studies, 10100 N Torrey Pines Road, La Jolla, CA, USA. (858) 453-4100. shaw@salk.edu.

AUTHOR CONTRIBUTIONS

Conception and design: P.E. Hollstein, R.J. Shaw

Development of methodology: P.E. Hollstein, L.J., Eichner, S.N. Brun, A.Kamireddy, R.U. Svensson

Acquisition of data (provided animals, acquired and managed patients, provided facilities, etc.): P.E. Hollstein, L.J., Eichner, S.N. Brun, A. Kamireddy, H. Galvez, R.A. Screaton, R. Berdeaux

Analysis and interpretation of data (e.g., statistical analysis, bio- statistics, computational analysis): P.E. Hollstein, L.J. Eichner, S.N, Brun, R.U. Svensson, M.N Shokirev, A. Williams, R.J., Shaw

Writing, review, and/or revision of the manuscript: P.E. Hollstein, L.J., Eichner, S.N. Brun, R.J. Shaw

Administrative, technical, or material support (i.e., reporting or organizing data, constructing databases): P.E. Hollstein, L.J., Eichner, S.N. Brun, L. Vera, D.S. Ross, T.J. Rymoff, A. Hutchins, R.J. Shaw

Study supervision: R.J. Shaw

Competing Financial Interests

None

deficient tumors. The SIK substrate CRTC2 was required for this effect, as well as proliferation benefits from SIK-loss.

Introduction

Twenty years ago, LKB1/STK11 was identified as the single gene responsible for the inherited cancer disorder Peutz-Jeghers syndrome [1] and soon after was discovered to be the third most frequent genetic mutation in non-small cell lung cancer (NSCLC), the leading cause of cancer deaths in the US and worldwide [2, 3]. Mutations in LKB1 are found in 20% of patients with NSCLC and frequently coincide with activating Kras mutations, prompting intense study of genetically engineered mouse models of LKB1 loss coupled with Kras activation to understand how deregulation of these two genes drives tumor formation and growth, and response to therapy in lung cancer [4–9]. Studies of human patients and genetically engineered mouse models have shown remarkable convergence in determining that Kras;LKB1 (“KL”) tumors show a unique tumor biology that is distinct and separable from other subtypes of Kras-driven NSCLC, such as tumors where Kras mutations are coincident with P53 loss [10]. One defining feature of KL tumors from a therapeutic standpoint is that these tumors exhibit primary resistance to a number of targeted therapeutics both in preclinical and human patients [4, 11], as well as very recent studies suggesting they are also uniquely resistant to immune checkpoint inhibitors, thus making LKB1-mutant lung cancer a very common form of cancer for which treatment options are extremely limited [12–14].

LKB1 encodes a serine/threonine kinase that activates a family of 14 downstream kinases including the AMP-activated protein kinase (AMPK), which collectively are known to control cell metabolism, cell polarity, and growth [15, 16]. Despite advances in the understanding of what the targets and functions of some of the downstream effectors of these 14 kinases are in different tissues, it remains unknown which of the 14 LKB1-dependent kinases are most required for its tumor suppressive activity in the lung. The best studied of these LKB1-dependent kinases is AMPK, which is a highly conserved master regulator of cell metabolism and growth that rewires metabolism and mTORC1 in response to low nutrient and energy conditions [16]. AMPK was hypothesized to be a lung tumor suppressor because it can indirectly suppress mTORC1 oncogenic signaling through the phosphorylation of a well-characterized downstream tumor suppressor, TSC2, and furthermore restrains pro-growth, pro-tumorigenic pathways that include inhibiting fatty acid synthesis needed for cell growth [8]. However, several recent studies utilizing mouse models of AMPK loss have suggested that AMPK plays a context-dependent role in cancer, as in some studies AMPK loss cooperated with mutational driver alterations in order to promote tumor formation in B- and T-cell lymphoma models [17, 18], but in opposite fashion, loss of AMPK became detrimental to cancer cell survival in the context of several leukemia models [19–21]. The requirement of AMPK for tumor cell survival fits with a wide body of literature on AMPK being required for cell survival under metabolic stress conditions, however, whether AMPK was pro- or anti-tumorigenic in the lung or any genetically engineered solid epithelial mouse model of cancer was completely unknown. In this context we recently examined whether AMPK would be the central target of LKB1 in

lung cancer [22]. Unexpectedly, we found that AMPK deletion in Kras-driven models of NSCLC did not mimic the effects of LKB1 loss, and instead suppressed tumorigenesis, being required for the outgrowth of Kras-dependent tumors. Therefore, the identity of the critical kinase(s) downstream of LKB1 responsible for its tumor suppressive functions in lung cancer remains unknown.

Mutational data in the TCGA database does not point to any of the 14 AMPK-related kinases (AMPKR) directly activated by LKB1 as being significantly mutated in lung cancer, and it has been assumed that redundancy among closely related kinases in this family could provide functional compensation, as nearly all of them contain one, two or even three very close homologs (see Figure 1A). Although the degree of compensation among family members is not well characterized, one possibility is that compensation in tumor suppressive functions among closely related AMPKR kinase family members masks their individual roles in tumor biology when analyzing their function in isolation, and thus may necessitate the disruption of multiple redundant family members to properly assess their role in tumor biology.

The salt-inducible kinases (SIK1, SIK2, SIK3) are three such redundant kinases among the 14 AMPKRs dependent on LKB1 for their kinase activity. The SIKs are best known to control gene expression through direct inhibitory phosphorylation of the transcriptional regulators class II histone deacetylases (HDACs) and the CREB-regulated transcriptional co-activators (CRTCs), thus controlling the transcriptional programs executed by these factors. The roles of SIK kinases in cancer remain very understudied. Among the SIKs, SIK1 had previously been described as a regulator of anoikis and suppression of metastatic potential in human breast cancer cells [23]. SIK2 was recently reported to play a pro-survival, oncogenic role in ovarian carcinoma cells [24] and to cooperate with SIK3 in promoting the survival of myeloid leukemia cells [25], indicating that like AMPK, perhaps SIK kinases can act in a pro-tumorigenic fashion and would not necessarily act as tumor suppressors; or at least exhibit context-dependent roles in different tissues. Most recently, the SIK kinases were shown to be critical targets inhibited by the oncogene GNAS through PKA-mediated phosphorylation. GNAS is mutationally activated in a subset of pancreatic adenocarcinomas and suppression of the activity of the SIKs appeared to be necessary for tumor maintenance [26], thus indicating that in certain tissues they exert growth-restraining properties. Whether the SIK kinases have functions in mediating effects of LKB1 in lung cancer has not been explored. Using a combination of cellular systems and genetically engineered mouse models, we analyzed members of the AMPKR family and report here the unexpected finding that the AMPKR kinases SIK1 and SIK3 cooperatively mediate important tumor suppressor functions of LKB1 in Kras-driven lung cancer in mice.

Results

CRISPR analysis of the AMPKR family in A549 cells

Which of the 14 kinases of the AMPKR family downstream of the LKB1 tumor suppressor are most critical for mediating its effects in NSCLC remains unknown, despite years of intensive study. Given the potential redundancies among different members within subfamilies of the AMPKRs, we sought a cellular system where the tumor suppressive

effects of LKB1 could first be modeled as a surrogate towards eventual genetic modeling of these kinases on lung cancer in the mouse. To begin this analysis, we chose the LBK1-null human lung adenocarcinoma cell line A549. A549 cells show no difference in their growth rates and doubling time in standard full media growth conditions when LKB1 cDNA is stably reconstituted (Figure S1A), yet show dramatic differences in tumorigenicity when orthotopically introduced into the lung by tail-vein injection (Figure S1B). We examined the expression of the 14 members of the AMPKR family in A549 cells with or without stable LKB1 reconstitution, which revealed detectable mRNAs of all AMPKRs except MARK1 (Figure 1A), indicating that many downstream kinases could be mediating the effects of LKB1 in these lung cancer cells. CRISPR/Cas9 was utilized to generate a panel of isogenic A549 cell lines, all of which bore stable retroviral reconstitution of wild-type LKB1 cDNA and were further genetically disrupted for different subfamilies of the 14 LKB1-dependent AMPKR kinases using single validated sgRNAs against each kinase via stable lentiviral expression. Lines were generated using multiple selectable markers to co-delete multiple members of each subfamily of AMPKRs. Immunoblotting confirmed loss of each AMPKR in their cognate cell line (Figure 1B–D), however SIK1 loss was confirmed via q-PCR due to lack of sensitive antibodies to robustly detect endogenous SIK1 under normal cellular conditions in human cells (Figure S1C). We additionally verified Sik1 disruption using Sanger sequencing and found a frequency of >80% in frameshift indels in the region surrounding the guide sequences in all cell lines targeted with Sik1 sgRNA guides (Figure S1D). Notably, despite not having an antibody to robustly recognize endogenous SIK1 under normal cellular conditions, we characterized a new antibody which recognizes the endogenous activation loop threonine phosphorylated by LKB1 in SIK1, SIK2, and SIK3 in human cells (Figure 1E) and show that this phosphorylation signal is correspondingly ablated in SIK KO cells. Additionally, as previously reported in other cell types [15], here in A549 cells lacking LKB1, there was no evidence of phosphorylation of the activation loop of any of the three SIK family members. CRISPR KO of SIK1 and SIK3 resulted in a modest increase in SIK2 P-T175 suggestive of cellular attempted compensation, although phosphorylation of CRTC3 was only modestly further bandshifted with loss of SIK½/3 as compared to SIK1/3 (Figure 1D,E).

Two features of epithelial cancer cells known to correlate well with *in vivo* tumorigenicity are the ability of cells to survive in suspension, indicative of anchorage-independent growth, and the ability of cells to form colonies when placed in 3D matrix. Indeed, we observed an LKB1-dependent suppression of growth in A549 cells plated in non-adherent conditions, yet no LKB1-dependent effect over the same time frame in growth on standard adherent conditions (Figure S1E **vs**. S1F, first two columns). Analysis of cells reconstituted with LKB1 that were subsequently targeted to disrupt subsets of AMPKRs revealed that loss of AMPKα1/α2, MARK¼, MARK2/3, NUAK½, BRSK½, or SNRK did not significantly alter the survival of A549 cells after 5 days in non-adherent conditions (Figure S1E). However, the combined loss of members of the SIK family showed a remarkable rescue of growth in non-adherent conditions, comparable to loss of LKB1 (Figure S1E). Notably, this was not observed in standard adherent conditions (Figure S1F).

We next examined colony formation in soft agar in A549 cells, which revealed a nearly 80% suppression of colony growth when LKB1 was reconstituted (Figure 1F,G). Unexpectedly, loss of AMPKa1/a2, NUAK½, MARK¼, MARK2/3, BRSK½, or SNRK did not afford LKB1-reconstituted cells the ability to grow in soft agar (Figure 1F,G). Analysis of all AMPKR subfamilies revealed very modest effects, except a remarkable full rescue of soft agar colony formation when the entire SIK subfamily was genetically disrupted. Further study with cells lacking each SIK family member individually or lacking pairs of the SIKs revealed that of the three SIK family members, SIK1 mediated the greatest single effect on soft agar colony formation (Figure 1F,G). Loss of SIK2 had a minor effect and loss of SIK3 in particular synergized with loss of SIK1 (Figure 1F,G). The relative importance of SIK1 and SIK3 to growth in soft agar matched the impact of SIK1, SIK2, or SIK3 loss on phosphorylation of CRTC3, one of the CRTC family of transcriptional coactivators that are targeted by SIK kinases (Figure 1D). Genetic disruption of SIK1 or SIK3 alone, but not SIK2 alone, resulted in an increased abundance of the faster mobility CRTC3 species (lower band), corresponding to a loss of phosphorylation. The observed redundancy among the three SIK family members matches what has been observed in studies of their function in mouse liver, where loss of all three unmasks strong phenotypes that are compensated when any one of the SIKs remains functional [27, 28]. Collectively, our findings in A549 cells suggest that the SIK subfamily, and particularly SIK1 may be playing an unappreciated role in lung cancer tumor biology.

Analysis of the role of the SIK family in genetic Kras dependent lung tumor models using CRISPR

Based on the findings in A549 cells, we sought to directly examine the role of SIK kinases in the well-studied genetic engineered mouse models of KrasG12D-dependent lung cancer [29]. Given a lack of readily available conditional floxed alleles of the SIKs, to assess the contribution of *Sik1* to tumor development, we first turned to a recently described lentiviral vector allowing for co-expression of Cre recombinase with Cas9 and an sgRNA of choice, pSECC [30]. pSECC lentiviruses can be delivered *in vivo* to the lungs of mice to induce CRISPR-mediated gene knockout in combination with Cre-mediated activation of oncogenes and deletion of floxed alleles in a single cell (Figure 2A). We began by generating pSECC vectors bearing three distinct validated RNA guides (sgRNAs) targeting *Sik1* (Figure S2A). We first tested effects of inactivating SIK1 via intratracheal delivery of functionally titered, equivalent amounts of pSECC viruses harboring sgRNAs against SIK1, along with sgRNAs targeting LKB1 (Figure S2B) and control sgTom (non-specific sgRNA) or sgLacZ [30, 31] sgRNAs, into KrasG12D mice containing a conditional Cre-activated reporter (ROSA26^{LSLluciferase}), which allows for real-time, non-invasive tracking of tumorigenesis and tumor progression occurring in these mice.

We quantitated tumor development using bioluminescence imaging (BLI) to measure the photon flux emitted from the lungs of these mice over time. This revealed significant acceleration of lung tumor development over the course of 22 weeks in mice treated with sgLkb1 (Figure 2B). All three cohorts of Kras mice treated with individual SIK1 sgRNAs displayed a modest, but consistent increase in tumor development over the control cohort by BLI over this time course. Of note, in a separate experiment we additionally tested the effect

of delivering pSECC viruses with two validated MARK4 sgRNAs in a parallel group of KrasG12D mice, and found that targeting *Mark4* alone in this model did not result in changes in tumorigenesis or progression in a distinguishable manner from control mice (Figure S2C).

In order to specifically gauge the effects of pSECC-SIK1 viruses in these mice, we quantitated their tumor burden as a percent of tumor area over the total lung tissue area by analysis of H&E stained lung sections of experimental and control cohorts (Figure 2C). Although we observed a wide variability in the overall tumor burden per mouse within all groups (Figure S2D), when considering all animals in each cohort as individual sets, as expected, sgLkb1-treated animals clearly displayed a significant increase in tumor burden (20% and 16% for sgLkb1 guides A and B, 0.9% and 1.3% for control sgTom and sgLacZ animals, and 4%, 2% and 2% for the Sik1 guides). Although the percent tumor burden on average was small in non-sgLkb1 animals at the 22-week endpoint, we corroborated the modest, but consistent fold change increase in the overall tumor burden of these mice with all three SIK1 sgRNA guides, ranging from 1.45–3.6 fold increase over the average of the control sgTom and sgLacZ cohorts.

To more closely examine the effects that disrupting *Sik1* had on tumors present in these mice, we analyzed the number and size of individual tumors in each mouse. Whereas the number of tumors per mouse did not reach above an average of n~9, among the non-sgLkb1 mice, the average size of individual tumors in all three cohorts of pSECC-Sik1 mice was significantly higher compared to control tumors, with a positive trend for all three guides used (8-, 3-, and 1.75 fold higher than control tumors for sgSik1 guides A, B, and C respectively (Figure 2D). These observations represented a skew towards a higher number of larger tumors in sgSik1-treated animals: 20% and 11% of tumors were larger than 1 mm^2 in mice with sgSik1-A and sgSik1-B vs 0% of controls, and 60% (sgSik1-A), 82% (sgSik1-B) and 70% (sgSik1C) of tumors were sized between 0.1–1 mm^2 compared to 42% for control tumors (Figure 2E). Thus, targeting SIK1 consistently yielded a larger tumor size on average in cooperation with KrasG12D activation.

Next, we aimed to assess the impact of deleting SIK1 with pSECC-CRISPR viruses in KrasG12D tumors that were also conditionally deleted for the tumor suppressor Trp53 (KP). Notably, genetic loss of LKB1 in the KP background (KPL) greatly accelerates the rate of lung tumorigenesis, tumor growth, progression, metastasis and tumor-related morbidity in mice compared to genetic KL and KP models [22]. We reasoned that loss of SIKs in a cell-autonomous P53-null setting may likewise provide a more permissive background to better reveal the potential tumor suppressive effects of SIK1 in models of NSCLC.

In addition to targeting SIK1 or LKB1 with pSECC in KP mice, we wanted to expand this analysis to include other SIK family members. We therefore developed sgRNAs to additionally target *Sik2* and *Sik3* (Figure S2B). BLI imaging across a 15-week time course revealed that in contrast to inactivation of SIK2 or SIK3, targeting SIK1 in KP mice resulted in an increased lung tumor burden compared to control mice (Figure 2F - SIK1 mice only) and (Figure S3A,B - SIK1–3 mice). Indeed, tumor burden quantitation from H&E-stained slides from the lungs of KP mice treated with sgSik1 guides at study endpoint showed an

average tumor burden of 23.7% (sgSik1-A), 16.1% (sgSik1-C) and 7.4% (sgSik1-B) guides compared to a burden of 4.6% and 7.1% of lung tumors induced by control sgTom or sgLacZ, respectively (Figure 2G). The percent lung tumor burden in mice targeted for SIK2 and SIK3 inactivation on average did not differ from the burden seen in control animals. In contrast, the average of all three cohorts targeting SIK1 with pSECC-sgRNAs in the KP model showed the percent lung tumor burden average to be 18% in sgSik1 animals from an average of 7.2% in control animals (a 2.5 fold change) (Figure S3C). At the individual level of KP mice treated with sgSik1 viruses, 5/10 animals showed tumor burden over 18%, which was the upper burden limit of control KP mice, and two individuals presented with burden of 38% and 39%, falling inside the range of tumor burden of KP mice treated with sgLkb1 guides (26–57%) (Figure S3D). Quantitation of individual lung tumors reveled that mice treated with viruses harboring all three sgRNAs targeting SIK1 resulted in a significantly larger tumor size compared to control-treated mice (Figure 2H). The range of tumors larger than 1 mm^2 in mice treated with sgSIK1 guides was 33%, 28% and 15% depending on sgRNA guide, compared to from 5% in control animals (Figure 2I). Nonetheless, considerable variability in tumor size was observed in these models, making us examine whether some of the sgRNAs were more effective than others at inducing disruption of the locus vivo, and/or whether a selection to observe out-of-frame indels in tumors at endpoint might be associated with specific guides. Using next generation deep sequencing of barcoded and pooled primary tumors, we observed a greater percentage of frameshift indels with Sik1 guide A, as compared to Sik1 guide B and C (Figure S3E,F), which correlated directly with the extent of tumor burden associated with these guides (Figure S3A). Similarly, the more effective LKB1 sgRNA, guide A, was also associated with a greater percentage of tumors bearing frameshift indels, indicative of a consistent selective advantage for tumors bearing LKB1 guide A (Figure S3E,F **vs**. S3A).

Analysis of genetic Kras-dependent lung tumor models using floxed *Sik1* and *Sik2* alleles

As a complementary and powerful alternative way to interrogate the function of SIK kinases in NSCLC, we turned to recently described conditional floxed alleles of *Sik1* [32] and *Sik2* [33] which we bred into the Kras-dependent mouse model to conditionally knock out expression of SIK1 and SIK2 (Figure 2J). We first confirmed that excising *Sik*1 floxed alleles in mouse liver resulted in the modulation of known LKB1-dependent transcripts (Figure S4A,B), corroborating some known CREB target genes in liver were induced by conditional deletion of this *Sik1* floxed allele. We next generated conditional floxed *Kras*;*Sik1* (KSik1) and *Kras*;*Sik2* (KSik2) mice and compared them against Kras (K) and *Kras*;*Lkb1* (KL) NSCLC models. Lung tumor induction by delivery of lentivirus expressing Cre-recombinase efficiently recombined *Sik1* and *Sik2* in lung tumors from the corresponding mice, and we further confirmed ablation of the expressed *Sik1* transcript in tumors from KSik1 mice (Figure S5A–B), which additionally displayed deregulation of known LKB1-regulated transcripts (Figure S5C–E).

KSik1 mice showed an acceleration in tumor growth over K mice (Figure 2K–L, Figure S6A–C), resulting in an increase from 8% to 12% in tumor burden over K controls (a 1.5 fold increase), which is within the range of tumor burden fold change observed in Kras mice treated with sgSik1 guides, although this did not reach statistical significance. Intriguingly,

3/13 animals presented with high tumor burden, and two of them (37% burden each) matched the level of tumor burden observed in KL mice (32%−56%) (Figure S6B), which was never observed in K mice, suggesting an estimation of about 15–20% of KSik1 mice displaying very high lung tumor burden. Surprisingly, genetic loss of *Sik2* did not increase - and instead slightly reduced - tumor burden compared to K mice, suggesting that SIK2 alone does not play a critical role in tumor suppression in the lung. Individual tumor analysis from KSik1 mice (Figure 2M, Figure S6D) revealed a highly significant difference in tumor size. 2% of tumors in K mice were larger that 1mm^2, whereas 9% of KSik1 tumors were this size or larger (Figure 2N).

Analysis of the role of the SIK family in genetic KP lung tumor models using floxed *Sik1* alleles

We next tested the effect of genetic ablation of SIK1 in the KP model of NSCLC. KPSik1 mice displayed an increase in tumor development compared to KP mice by BLI (Figure 2O, Figure S7A–B). Despite variability in tumor burden among individual mice (Figure S7C), 2/5 mice reached tumor burdens of 41–42% of the total lung area, which is similar to the tumor burden range of KPL mice (46%−62%) whereas KP mice had smaller burden (1–27%) (Figure S7D). As a cohort, KPSik1 mice showed an increase from 10% to 28% in tumor burden over KP mice, (a 2.8-fold increase) compared to a tumor burden of 52% in the KPL mice (5.25-fold increase over KP) (Figure 2P), and this was consistent with the results observed in KP mice treated with SIK1 sgRNA guides (Figure S3B, 2.5 fold tumor burden increase of KP+sgSik1 over KP+sgControls). Analysis of individual tumors in KPSik1 mice however showed a significant increase in tumor size in these mice compared to KP (Figure 2Q), and loss of SIK1 in this model increased the percentage of tumors larger than 1 mm^2 (18% tumors in KPSik1 vs. 7% in KP), and furthermore 2% of tumors in KPSik1 mice were (>10 mm^2) (Figure 2R).

To further ascertain the cell biological effect of SIK1 loss in lung cancer cells, we derived (n=3) cells lines from KPSik1 tumors, first confirming that they expressed no detectable *Sik1* transcript (Figure S8A), and functionally compared them to matched KP lines (n=4) derived from the same genetic background. KPSik1 cells displayed an enhanced ability to form colonies from single cells in 2-D culture compared to control KP cells, and moreover grew into significantly larger colonies (Figure S8B–D). We next tested the ability of these cells to grow colonies in soft agar, and found that KPSik1 cells displayed an enhanced ability to grow both more and larger colonies in soft agar compared to KP cells (Figure 2S and Figure S8E). Lastly, we tested the dependency of SIK1 loss on the growth of these cells, and found that re-expression of the SIK1 cDNA significantly reduced their proliferative capacity (Figure S8F).

Targeted co-inactivation of SIK1 and SIK3 accelerates tumor growth in Kras-driven NSCLC

Despite the enhanced tumor growth phenotype resulting from inactivation of SIK1, the loss of any individual SIK family kinase did not fully recapitulate the tumorigenic potential of LKB1 loss in our mouse models. SIK1, SIK2 and SIK3 share common substrates and therefore, it is likely that functional redundancy from the remaining SIK family members may mask the ability to further reveal LKB1-like effects on tumor growth upon loss of an

individual SIK kinase, in agreement with our observations of targeted loss of SIK1 versus combinations of SIK1+3 and SIK1+2+3 loss in A549 cells (Figure 1D–F). To test this hypothesis *in vivo*, we combined our genetic floxed KSik1 model with pSECC-mediated inactivation of SIK3 (Figure 3A). This model uses Cre recombinase to activate Kras and inactivate SIK1, and simultaneously delivers CAS9 and a sgRNA targeting SIK3 (sgSik3-B). Thus, this system effectively inactivates SIK1 and SIK3 simultaneously. Mice with this genetic combination efficiently yielded tumors that were deleted for *Sik1* and further showed disruption of reading frames at the *Sik3* sgRNA target site (Figure S9A–E). Remarkably, compounding the loss of these two SIK family members accelerated tumor growth as compared to K+sgTom mice or to cohorts that inactivated SIK1 or SIK3 singly, either using the genetic model (KSik1) or CRISPR-based targeting with sgRNAs targeting SIK1 or SIK3 (Figure 3B–D, Figure S9B). Floxed KSik1 mice treated with pSECC-sgTom displayed an intermediate acceleration of tumor growth between KSik1+sgSik3 and K +sgTom mice, which was comparable to inactivation of *Sik1* with sgRNAs. Furthermore, BLI imaging showed that all three conditions targeting SIK1 alone resulted in enhanced tumor growth in mice as compared to targeting SIK3 by itself. At study endpoint, tumor burden quantitation showed that KSik1+sgSik3 mice showed a significantly higher burden (10%) over control mice (1%), which was further reinforced upon tumor size quantitation (Figure 3E,F). Use of deep sequencing of tumors to analyze the frequency of frameshift indels in the tumor DNA revealed a strong selection for LKB1 sgRNA guide A (Figure S9C,D), similar to before (Figure S3E). However now the increased percentage of tumors bearing a high proportion of frameshift indels could be clearly observed for the Sik3 sgRNA B, strikingly only in the Kras Sik1 mice and not in Kras mice alone (Figure S9C,D). We interpret these results as potential evidence for a selective advantage of tumors inactivating Sik3 only when they already lack Sik1.

Despite an apparent lower total tumor burden in the cohort of KSik1+sgSik3 mice compared to K+sgLkb1 mice (Figure S9F,G), the average size of individual tumors between K+sgLkb1 and KSik1+sgSik3 mice was instead comparatively similar (average size >1 mm^2, difference in means between these two cohorts not significant) and both were significantly larger than tumors from control K+sgTom mice (Figure 3F). Notably, mice with these two genotypes were the only ones with average size tumors above this threshold among all cohorts tested. We reasoned that enhanced cellular proliferation rates may underlie the dramatic increase in tumor size observed in these cohorts. BrdU positivity analysis showed that KSik1+sgSik3 tumors showed the highest average percent of BrdU incorporation among all cohorts tested (Figure 3G), indicating that inactivation of multiple SIK kinases resulted in higher numbers of proliferating cells per tumor compared to control or single SIK-deleted tumors. Correlated with these observations, tumor size distribution analysis showed that KSik1+sgSik3 mice presented with the largest percent of tumors >10 mm^2 among cohorts (9% of tumors of this genotype, 5% observed in K+sgLkb1, 2% in KSik1 mice, 0% in all other cohorts) (Figure 3H). Together, our data indicate that the combined inactivation of SIK1 and SIK3 yielded a tumor phenotype characterized by a high percentage of actively dividing cells, resulting in an expanded fraction of large tumors similar in size to those observed upon loss of LKB1. We additionally assessed whether Sik1+3 loss would recapitulate the reported association of LKB1 loss with an elevated recruitment of tumor-associated neutrophils, a hallmark of *KL*

lung adenocarcinomas [11]. Using immunohistochemistry for the neutrophil marker Ly6G, we observed a significant increase in the percentage of neutrophils present in the KL tumors as compared to K tumors, and moreover this increase in neutrophil staining was also mirrored in the KSik1/3 tumors (Figure S9E). Together these results suggest that loss of SIK1 and SIK3 in the mouse recapitulates histological aspects of LKB1 loss in both tumor size and immune phenotype.

SIK-mediated control of gene expression

To determine which transcriptional programs driven by LKB1 inactivation are under the control of the SIKs, we performed transcriptional profiling using RNA-sequencing on primary tumors plucked from K+Pgk-Cre and K+pSECCsgTom (**K**), (KSik1+Pgk-Cre) (**KSik1)**, KSik1+pSECCsgSik3-B (**KSik1+3**), and K+pSECCsgLkb1-A (“**KL-A”**) genotypes. Clustering all genes across all genotypes revealed discrete clusters of genes that were clearly co-regulated in KL-A and KSik1+3 tumors (Figure S10A). Expanding these clusters (Figure S10A, red and green boxed insets), it is evident that SIK1+3 deletion induced the same magnitude of transcriptional deregulation as LKB1 inactivation, suggesting that the SIKs are the main targets of LKB1 in the normal suppression of these two specific subsets of genes. Notably, these clusters did not show deregulation in KSik1 tumors (Figure S10A), suggesting that coincident inactivation of SIK1+3 is necessary to reveal the LKB1-dependent transcriptional programs that are under SIK-mediated regulatory control. Moreover, when we unbiasedly clustered the data from K, KSik1+3 and KL-A tumors across all genes and samples, the samples clustered cleanly by genotype, confirming that genotype-dependent transcriptional changes dominated the dataset (Figure 4A).

We next used differential expression analysis (FDR <0.05, +/− 1.5 fold) to define a KSik1+3 gene signature as compared to K tumors and, independently, a KL-A gene signature as compared to K tumors. We then identified the overlap between the KSik1+3 and KL-A gene signatures. 344 (38%) of the genes within the KL-A signature that were upregulated in KL-A tumors were also significantly upregulated in KSik1+3 tumors. Similarly, 627 (41%) of the genes with the KL-A signature that were downregulated in KL-A tumors were also significantly downregulated in KSik1+3 tumors (Figure 4B). Together, we identified 971 genes commonly regulated by LKB1 or SIK1+3 inactivation (Figure 4C). This data suggests that SIK1 and SIK3 together may be responsible for ~40% of the transcriptional changes induced upon LKB1 loss in primary lung tumors.

We used Gene Set Enrichment Analysis (GSEA) to unbiasedly explore the pathways regulated by SIK1+3. We considered the comparison of KSik1+3 tumors to K tumors, and queried this data against the “Hallmark” group of gene sets using GenePattern. We performed the same analysis considering KL-A tumors compared to K. We then compared the top enriched gene sets to determine which LKB1-dependent processes may be mediated by SIK1+3. Two gene sets related to well-established hallmarks of LKB1 mutant lung tumors, “Epithelial Mesenchymal Transition” (EMT) and “IL-6 JAK Stat3 Signaling,” were among the top enriched gene sets, 1st and 8th, respectively, in the KSik1+3 data (Figure 4D). In the KL-A data, these gene sets were the 6th and 7th most enriched. Metascape pathway analysis of the 344 genes upregulated in both KL-A and KSik1+3 tumors (Figure 4B)

confirmed a role for SIK1+3- and LKB1-dependent deregulation of the IL-6 pathway, in that "interleukin-6 family signaling" was identified as the second most significant term (Figure S10B). We combined the enriched genes from the GSEA plot with the genes comprised in the Metascape term to create an IL-6 Signaling gene list, shown in a heatmap (Figure 4D). The enriched genes from the EMT gene set are also depicted in a heatmap (Figure 4D). Thus, transcriptional analyses suggest that loss of SIK1+3 replicates effects on EMT and IL-6 signaling pathways that are induced by LKB1 loss in lung tumors.

We then extended our analysis of the 344 genes upregulated in both KL-A and KSik1+3 tumors (Figure 4B). We queried this gene list in Enrichr. IL6 signaling or related Jak-STAT signaling were the top enriched pathways within this gene list across KEGG, WikiPathways, Reactome and BioCarta analyses (Figure 4E, Figure S10C). This further implicates SIK1+3 in the regulation of the IL6 pathway. Homer motif enrichment analysis identified one statistically significant motif ($p < 1e-12$) within the promoters, defined as +/−2kb of the transcriptional start site (TSS), of the 344 upregulated genes (Figure 4F, top motif). This motif includes the recognition motif for the AP-1 family of transcription factors, including AP-1, JUND, FOS, FOSL1, and FRA2. Alignment of this motif to the JUND motif is pictured (Figure 4F). This suggests that the AP-1 family of transcription factors may be involved in driving a portion of the LKB1- and SIK1+3-dependent transcriptional changes.

A key established target of the SIKs is the CRTC family of transcriptional coactivators of the CREB transcription factor, and has also been reported to control AP-1 activation (38, 39). We found that both AP-1 and CREB-dependent transcription became chronically upregulated by SIK1- or LKB1-dependent loss in cultured mouse and human NSCLC cells, in correlation with bioinformatic analysis of mouse tumors (Figure S10D–G, Figure S11A–D). To query this bioinformatically, we searched the promoters of the 344 upregulated genes common to KL-A and KSik1+3 tumors for AP-1 and CRE motifs. 74% of genes have at least one motif for CREB (CRE), AP-1 (AP1) or both in the promoter (Figure S10D). It follows that the genes involved in the biological processes that are deregulated upon LKB1 and SIK1+3 loss, including EMT and IL-6 signaling, are likely to be under transcriptional control by the transcription factors whose activity are modulated in these conditions, potentially CREB and AP-1. Indeed of the 344 genes commonly upregulated in murine Kras tumors by LKB1 loss and SIK1+3 loss, 55 genes contain both predicted elements in their promoters (Figure 4G), 31 contain CRE elements (Figure S10E), and 170 contain AP1 elements (Figure S10F). While only some of these motifs are likely to be functionally bound by CREB or AP-1 in primary lung tumors, this data suggests that both CREB and AP-1 may be involved in regulating a subset of the genes upregulated upon LKB1 and SIK1+3 loss. One well-studied promoter that contains functional AP-1 and CREB binding is that of IL-6 [34]. As the enrichment analysis suggested, FPKM plots of the RNA-sequencing data from each tumor per genotype reveals transcriptional upregulation of nearly all steps of the canonical JAK/STAT pathway, from cytokines (IL-6, IL-33) to receptors (IL4RA, Osmr), core components (JAK3, STAT1, STAT3), coactivators (Bcl3), and well known STAT targets (SOCS3) **(Figure 4H)**. Thus, our data support the model that LKB1 loss in lung tumors induces IL-6 signaling through inactivation of SIK1+3.

To assess the overlap between the changes in gene expression by loss of Sik1+3 deletion in mouse tumors and genes regulated by loss of LKB1 in human cells, we used GSEA to query the top 500 upregulated genes in Sik1+3 tumors and compared them against a ranked list of all genes differentially regulated by the presence or absence of LKB1 in human NSCLC A549 cells based on RNAseq expression profiling (from A549-pBabe or A549+LKB1 cells represented in Figure 1 and Figure 5). We found there was a significant enrichment of genes upregulated in mouse tumors by Sik1+3 loss that were also found to be upregulated in human A549 cells compared to LKB1-reconstituted cells (Figure S10G, graph and 1st line in the summary table), which notably included IL6 and IL33. We also queried the set of 344 genes that were upregulated in common by Sik1+3 loss and Lkb1 loss (Figure 4B) to ask whether the set of genes that were commonly regulated by Sik1+3 loss and Lkb1 loss in mouse tumors were also regulated by LKB1 in human NSCLC cells. GSEA analysis showed a significant enrichment of this gene set when comparing genes differentially regulated by LKB1 in A549 cells (Figure S10G, 2nd line in the summary table). Furthermore, this gene set was also found to be enriched in differential transcriptional profiles generated by RNAseq of two other human NSCLC lines that we queried (H1355, H157) in the LKB1-null state vs. LKB1 cDNA re-expression (Figure S10G), collectively indicating that Sik1+3 loss in mouse tumors induces transcriptional changes that are mirrored in part by Lkb1 loss in the mouse and by LKB1 loss in human cells. These included genes associated IL-6 pathway signaling, which further raised the possibility that LKB1 may control IL-6 signaling through SIK1/3 in human NSCLC cells.

SIKs control IL-6 and STAT signaling via CRTC2

To further explore whether the gene expression changes seen were due to cell-autonomous effects of loss of SIK1/3 signaling on transcription within the tumor cells themselves, as compared to elevated cytokine signaling in surrounding stroma or immune cells, including the elevated presence of tumor-associated neutrophils present in the microdissected tumors, we turned to human A549 NSCLC cells in culture. Picking a limited number of well-known SIK1-regulated mRNAs (*NR4A1, PDE4B*), we examined a limited number of genes in the cytokine/JAK-STAT signaling pathway deregulated in the KL and KSik1/3 tumors. As seen in Figure S12A, mRNAs of some cytokines and cytokine receptors (IL-10, IL-15, OSMR) were suppressed by LKB1 reconstitution in A549 cells, and were largely reversed by Sik1/3 deletion in LKB1-expressing cells.

As IL-6-dependent signaling has been shown to be a common feature of other LKB1-deficient contexts [35], we examined the cell-autonomy of LKB1 effects on IL-6. As a first examination, we created Lkb1 or Sik1/3 CRISPR KO in murine KP cell lines using independent combinations of sgRNA guides targeting Sik1 and Sik3 in two independent KP lines, and profiled IL-6 production by ELISA. In these cells, we observed significantly elevated IL-6 production in both the Lkb1-deleted and Sik1/3-deleted KP cells (Figure 5A). We next examined IL-6 production in A549 cells with and without LKB1 reconstitution or SIK1/3 CRISPR deletion. Notably, A549 cells produced IL-6 basally, which was strongly inhibited when LKB1 was restored (Figure 5B), and this effect of LKB1 reintroduction was fully reversed upon deletion of SIK1/3.

Given the presence of CRE and AP-1 binding motifs in the IL-6 promoter [34], we next examined whether CRTC family members may mediate effects of LKB1- or SIK1/3 on IL-6. First we examined mRNA expression levels of the three members of the CRTC family in murine KP tumors as well as in A549 cells from RNA sequencing data. In both mouse (Figure S12B) and human (Figure S12C) Kras mutant lung adenocarcinoma cells, CRTC2 was the most prominently expressed family member. Using two distinct sgRNAs, CRTC2 was deleted in A549 cells bearing LKB1 reconstitution and SIK1/3 deletion, which resulted in complete suppression of IL-6 production (Figure 5B). Given this requirement of CRTC2 for IL-6 production, we examined whether gene expression controlled by SIK1/3 loss might similarly be dependent of CRTC2. We observed partial or full dependence on CRTC2 amongst genes well known to be CREB targets (NR4A2, NR4A3), but also amongst cytokine signaling (IL-33, STAT1) and proliferation genes (AREG, EREG) (Figure 5C). To examine whether these elevated mRNAs would translate into altered signaling pathways, we examined total STAT1 protein levels in our A549 cell series. A549 cells expressed STAT1 protein, which was reduced by LKB1 reconstitution, but that effect of LKB1 was reversed by SIK1/3 deletion (Figure 5D, Figure S12D). The increase in total STAT1 protein (both α and β splice isoforms induced by loss of SIK1/3 was in turn reversed by deletion of CRTC2. In addition, SIK1/3 loss in the LKB1-proficient cells not only resulted in elevated STAT1 proteins but also increased basal phosphorylation of STAT1 at Y701 (Figure 5D, Figure S12D), perhaps due to autocrine cytokines also being produced in parallel with STAT1 upon Sik1/3 deletion. This too was reversed by CRTC2 loss (Figure 5D).

We next examined whether CRTC2 was also a key target of Sik1/3 loss on growth in anchorage-free settings. First we returned to growth and anoikis survival in detached conditions, and as observed earlier (Figure S1E), LKB1 re-expression of LKB1 in A549 cells reduced their growth and survival in detachment, which was largely reversed by Sik1/3 loss,and this added growth from Sik-deficieny in detacted conditions was suppressed by CRTC2 loss (Figure 5E). The enhanced growth in soft agar induced by SIK1/3 deficiency was also diminished by CRTC2 deletion (Figure 5F), indicating that CRTC2-dependent control of transcription may be a major target of LKB1- and SIK1/3-dependent tumor suppression.

Sik-mediated effects are largely LKB1-dependent

As we and others have previously demonstrated, despite LKB1 being a predominant upstream kinase for AMPK in most tissues types, most cells types also use CAMKK2 as an upstream kinase for the same activation loop threonine that LKB1 phosphorylates, providing residual AMPK activity in LKB1-deficient cells, tumors, and tissues [36]. Now armed with better tools and clear effects on a number of readouts, we sought to examine whether Sik family kinases might also retain catalytic activity independent of LKB1. Our first hint this was not the case came from use of the new activation loop threonine phospho-specific antibody which recognizes endogenous Sik1, SIK2, and SIK3 in A549 cells (Figure 1E). Despite an apparent absence of P-SIK1, SIK2, or SIK3 in the A549 cells which lack LKB1, we wondered if an alternative kinase might be upregulated under detached conditions, given that this is a critical context for the SIKs and LKB1 activity. We next performed immunoblotting analysis to profile a number of targets of LKB1 and AMPK in A549 cells

with or without LKB1 add-back, and/or with Sik½/3 deletion (Figure 5G). This analysis again found no evidence of residual P-SIK1, SIK2 or SIK3 in A549 cells without LKB1 restoration, unlike P-AMPK, which was still residually phosphorylated in A549 cells, particularly in detached conditions, as was the AMPK substrate P-Raptor (Figure 5G). Furthermore, we performed in vitro kinase assays on Sik1 and Sik3 isolated from LKB1-containing or LBK1-deficient A549 cells, revealing a complete loss of Sik1 and Sik3 catalytic kinase activity in the LKB1-deficient cells, consistent with the activation loop threonine being required for catalytic activation of these kinases (Figure S13A–D). To functionally address whether SIK1 and SIK3 may have tumor suppressor functions independent of LKB1, we used A549 cells targeted for deletion of these kinases individually or the Sik1/3 dual combination and performed soft agar colony formation. First, with single disruption of SIK1, or SIK2, or SIK3, there was no statistical increase colony number in the LKB1-deficient cells (Figure S13E), unlike the benefit of SIK1 loss on soft agar colony formation in the context of A549s bearing LKB1 (Figure 1F,G). However, a modest increase (~ 1.8 fold) in soft agar colony formation was observed when SIK1 and SIK3 were both removed from A549 cells (Figure S13F), compared to >4.5 fold increase in colony formation in the LKB1-replete A549 cells (Figure 1F). The observed increase in soft agar colonies when SIK1/3 are deleted in LKB1-null cells raises the possibility that these kinases may have some LKB1-independent scaffolding functions, or roles not reliant on SIK1/3 kinase activity in these cells.

Discussion

Here we have made the unexpected finding that the AMPK-related kinases SIK1 and SIK3 redundantly mediate some of the tumor suppressor activity of LKB1 in Kras-driven lung cancer. Notably, head-to-head analysis of the 14 LKB1-dependent AMPK family kinases in A549 cells revealed a unique role for the SIKs in suppressing soft agar colony formation as well as susceptibility to cell death in detached conditions. In both assays, combined SIK1/SIK2/SIK3 deletion gave a phenotype most similar to LKB1 loss, and none of the other AMPKR subfamilies gave rise to similar effects on soft agar colony formation or growth in detached conditions. Indeed, our previous genetic studies in mice indicate that AMPKα1 and α2 do not play a conventional tumor suppressor role in Kras driven lung tumors and when deleted result in decreased tumor burden, in stark contrast to the robust tumor increases in models from loss of LKB1 [22]. In both K and KP models of NSCLC, loss of SIK1 accelerated tumorigenesis, albeit in a manner not fully penetrant to phenocopy LKB1 loss. It is worth noting that p53 and LKB1 are mutually exclusively mutated in the context of lung adenocarcinomas with Kras mutations in human patients so the KPL mouse model is simply an additional tool for examining effects of LKB1 tumor suppressor activity. Interestingly, LKB1 is co-mutated with p53 in human adenocarcinomas with wild-type Kras, so this is a context worth exploring further in mouse models to define SIK-dependent effects in.

Notably, the K and KP models with pSECC-induced models targeting the Siks or Lkb1 only generated adenocarcinomas and we did not observe an increased incidence of squamous cell carcinoma (SCC) or adeno-squamous transdifferentiating lesions at the histological level. An increased incidence of squamous cell carcinoma cell has been reported as a hallmark of

LKB1 loss in some mouse models [5, 6, 9, 37, 38]. While the reasons for this discrepancy are not resolved, we believe that some contributing factors could be potential differences in latency of tumor development at experimental endpoint among different models, the choice of strain background, or the use of lentiviral Cre, which is thought to favor the incidence of adenocarcinoma development in models of KRas/Lkb1 over adenoviral Cre [39] which may influence the frequency at which histologically defined squamous carcinomas may be able to develop and be detected in these models.

Here we found that concomitant loss of SIK1 and SIK3 in Kras mutant tumors further cooperatively accelerated lung tumorigenesis, and promoted the ability of tumors to grow comparably to those observed by loss of LKB1 (Figure 3). Furthermore, the loss of SIK1/3 recapitulated the reported phenotype observed in LKB1 mutant tumors denoting a significant accumulation of neutrophils within tumor areas. In our studies, we observed over a 3-fold increase in the number of infiltrating neutrophils in both Lkb1- and Sik1/3 targeted tumors when compared to tumors from KRas control mice by histological quantification of the neutrophil marker Ly6G. An LKB1-dependent increase in tumor-associated neutrophil infiltration has been thought to contribute to the establishment of a pro-inflammatory, pro-tumorigenic state in lung tumors bearing LKB1 mutations, and is characterized by an increase in the production and secretion of IL-6 by tumor cells, which attracts neutrophils that are thought to exert immunosuppressive effects [11]. Future studies are needed to determine whether additional co-deletion of *Sik2* or a distinct AMPKR might further enhance the SIK1/SIK3 tumor and immune phenotypes. It will also be interesting to examine how combined floxed alleles of *Sik3* might synergize with loss of SIK1 and activation of Kras in the lung, since pSECC targeting is not fully penetrant [30] (Figure S9C,D), and thus may limit the amount of synergistic signal that loss of SIK3 could provoke in this study. Independently, in elegant studies using CRISPR gene-editing in Cas9-expressing mice, Murray and colleagues have also found cooperating roles for Sik1 and Sik3 as arbiters of tumor suppression in NSCLC [40]. Together, these studies underscore critical functional roles which these two kinases share in mediating LKB1's tumor suppressive function in the lung.

Functional analysis of the three SIK genes in mammals has largely come from studies of their roles in metabolic tissues such as liver, adipose, and muscle, where they are known to phosphorylate and inhibit the CRTC family of transcriptional co-activators as well as the Class IIa family of histone deacetylases [27, 28, 32, 41–43], effects we observed here in A549 NSCLC cells (Figure 5G). Studies of the role of the SIKs in different metabolic processes in metabolic tissues has been performed in genetic knockout mice and in cell culture systems, but the roles of the SIKs in tumor cells is very underexplored. However, there are hints in the literature that SIK1 and/or SIK3 may behave as tumor suppressors in some contexts. Notable very recently, biochemical inhibition of the SIK subfamily was found to be a key driving force of PKA-dependent signals from oncogenic GNAS in pancreatic cancer [26]. Moreover, an early shRNA screen for kinases involved in colony formation and tumorigenesis in mammary epithelial cells reported SIK1 as one of the top hits of the screen [23]. Depletion of *Sik1* using shRNAs or expression of a kinase-dead SIK1 led to increased metastatic spread in a transplant model, which was paralleled by TCGA data

showing that reduced *Sik1* mRNA correlated with poor clinical outcomes in breast cancer [23].

Given that the main study of the SIKs to date has been in metabolic tissues for their role in controlling transcriptional regulators, we performed transcriptional analysis on primary tumors from Kras mice alone or those bearing loss of LKB1 or SIK1 and SIK3. Transcriptional profiling of primary tumors revealed that loss of LKB1 and loss of SIK1/3 in Kras lung tumors trigger highly overlapped transcriptional responses, with 38% of the genes upregulated from LKB1-deficiency being upregulated by SIK1/SIK3 loss. Given that LKB1 activates 12 kinases in addition to SIK1 and SIK3, it is surprising that loss of just those two kinases would trigger such an overlapping extent of gene expression. Analysis of the 344 genes upregulated in common between LKB1 and SIK1/3 loss revealed many promoters bearing CREB and AP-1 binding sites. Notably, both AP-1 and CREB-dependent transcription have been tied to tumorigenesis before. Notably**,** studies on roles of the CRTCs, perhaps the best-established substrates of the SIKs, have been common in a specific type of mucoidal epithelial (MEC) tumors caused by translocations involving hyperactivation of CRTC function. Increased expression of both CREB and AP-1 target genes has been studied in this tumor context extensively [44]. In some of the initial studies identifying the CRTC proteins, it was noted that the phorbol ester TPA can cause nuclear translocation of CRTC1 [45] and that deletion of the AP-1 binding sites in the IL-8 promoter resulted in it being no longer responsive to CRTC1 [46]. Subsequent studies directly showed that CRTC1 is a co-activator for AP-1 and its regulation of some AP-1 targets is independent of any effects on CREB [44]. Importantly, overexpression of CRTC1 synergized with c-Jun overexpression to drive growth in HeLa cells (which are LKB1-deficient), and siRNA to CRTC1 blocked the ability of overexpressed c-Jun to induce BrdU staining, directly implicating CRTC1 in cell proliferation [44]. Indeed we observed elevated BrdU in the SIK1/SIK3 deficient tumors and colony formation in SIK1-deficient KP cells was greatly enhanced as well (Figure 3F). Besides AP-1 dependent effects on proliferation, recent studies of the CRTC1-MAML2 fusion in MEC tumors have found that CRTC1-dependent induction of AREG, an EGF family ligand, occurred in a manner dependent on CREB binding the AREG promoter [47] and AREG-dependent activation of EGFR was important for the tumorigenic potential of CRTC1-MAML2 fusion proteins in MEC tumors. Indeed treatment of such tumors with the EGFR monoclonal antibody Cetuximab blocked growth in xenografts [47]. Given the importance of AREG-EGFR to proliferation of these MEC tumors, it is notable that we find *AREG* is upregulated in this study in a LKB1-deficient tumors in a SIK1/3-CRTC2 dependent manner. In addition, another CRTC transcriptional target, *NEDD9*, was recently reported to be important for LKB1 tumor suppression [48]. Epithelial-Mesenchyme Transition was another well-noted LKB1-dependent effect on gene expression [49], and is also highly upregulated in the SIK1/SIK3-deficient tumors.

The single most common biological pathway upregulated at the mRNA level in common between LKB1 loss and SIK1/SIK3 loss was IL6/JAK/STAT signaling. Very recently, two studies describing conditional models of Peutz-Jeghers syndrome (PJS), the cancer predisposition syndrome exclusively driven by congenital mutations in LKB1, have drawn a consistent connection between LKB1 deficiency and upregulation of the IL6/JAK/STAT

pathway in different lineages [50, 51]. Loss of LKB1 in T cells or intestinal stromal cells resulted in the secretion of IL6/IL11 cytokines, which in turn drove hyperactivation of the JAK/STAT signaling in the stromal compartment of the intestine required for tumor growth. One group furthermore found that reduced expression of SIK1, MARK1 or MARK4 in fibroblasts was sufficient to induce production of IL-11 [50], which suggests that control of this pro-inflammatory axis may be a common target of SIK- and LKB1-dependent regulation in multiple tissues and cell types. We show here in both murine and human lung adenocarcinoma cell lines that SIK1/3 deletion provokes IL-6 production to a similar extent as LKB1 deletion, and IL-6 production is ablated if CRTC2 is deleted (Figure 5A, B). It will be important to investigate whether inhibition IL6/JAK/STAT pathway could have therapeutic value in LKB1-mutated lung cancer, especially given that therapeutic options are so limited for this tumor type. Furthermore, it will be interesting to determine if additional genes within our newly-defined list have as-of-yet unexplored targetable potential.

Mechanistically, it is also noteworthy that both SIK1 and SIK3 were previously reported to regulate TLR4 signaling to NFkB via direct binding and regulation of TRAF6 [52]. Whether CREB, AP-1, NFkB, or STAT-dependent gene expression underscores the primary resistance seen in KL mouse models and striking resistance to immune checkpoint inhibitors seen patients with LKB1 mutations remains to be determined, but several specific hypotheses can now be tested in future studies.

While unexpected, the finding that SIK1 and SIK3 mediate much of the tumor suppressor function of LKB1 also opens new avenues of therapeutics aimed against the pathways directly regulated by SIK1 and SIK3. Given that only a handful of substrates are known for SIK1 and SIK3, there is much to be learned mechanistically about their function in lung cancer, which may have broad implications for resistance to checkpoint inhibitors and the large fraction of NSCLC bearing LKB1 mutations for which there are currently no robust therapeutic strategies.

Materials and Methods

Cell Culture and cell lines

All cell lines were maintained in DMEM supplemented with 10% FBS and incubated at 37°C with 5% CO_2. All cell lines were mycoplasma tested once a month. A549 cells were from ATCC, and isogenic A549 lines reconstituted with pBABE-LKB1 WT were obtained by retroviral transduction under selection (hygromycin, 600ug/mL). 634T KP cells were a gift from Kwok Wong. FVB-mouse lung tumor-derived KP and KPSik1 cells were isolated from freshly collected mouse tumors, minced and digested with 1mg/ml collagenase/dispase (Sigma) in DMEM+10% FBS and 1x Penicillin/Streptomycin for 2hrs under rotation at 37°C, and were subsequently cultured on DMEM with 10% FBS, 1x penicillin/streptomycin (Gibco) and 2.5ug/ml fungizone (Gibco), with media replacement every 48hr over 6 days to establish sterile cultures. KPSik1 tumor-derived cell lines were confirmed to be SIK1 KO by qPCR of *Sik1* transcript. Luciferase assays: 634T cells stably expressing sgTom, sgLKB1 and sgSIK1 guide RNAs were transfected with plasmids encoding AP1 target promoter and CREB-binding CRE promoter reporters (Cignal CRE (CCS002L), AP1 (CCS-011L) coupled to luciferase, according to the manufacturer's instructions.

In vitro Kinase assay

Flag-tagged SIK1 cDNA - WT or Threonine 182 activation-loop mutant (TA), or SIK3 WT or TA-mutant were expressed in A549-pBabe cells or A549-LKB1 reconstituted cells with pLenti-Neo. Equivalent amounts were immunoprecipitated (Sik1, FLAG-M2-resin, SIK3, Bethyl A302–455A with Protein A beads) from cell lysates (3mg/sample). SIK activity was performed in a final volume of 50ul containing 15 ul bead volume of protein kinase and 35ul of reaction mix, using 200 uM of Sakamoto-tide (CRTC2 peptide ALNRTSSDSALHRRR) (MRC-PPU Reagents) as a substrate, with 50 mM HEPES, 1 mM EGTA, 10 mM magnesium acetate and 2 uM [γ^{32}P]-labelled ATP. Control reactions lacked kinase using control immunoprecipitates, or lacked Sakamototide in the presence of immunoprecipitated kinase. Reactions were incubated at 30 degrees for 20 min, and were terminated by spotting 40ul of reaction on P81 phosphocellulose paper followed by immediate immersion in 75M orthophosphoric acid. Papers were washed three times for 10 min with 75mM orthophosphoric acid, and one final wash for 5 minutes in acetone. Papers were air-dried, and incorporation of P32 was quantitated by Cherenkov counting.

Soft Agar Colony Growth Assay.

0.02 million KP/KPSik1 or 0.03 million A549 cells were mixed with agarose in 2x growth medium (final concentration 0.3%), plated on top of a solidified layer of 0.6% noble agar in 6 well plates and fed every 4–5 days with growth medium. Cell were collected after 3 weeks, stained with 0.02% Giemsa (Sigma-Aldrich 48900) for 10 minutes at room temperature, then washed with PBS and stored at 4 degrees overnight for stain development. Plates were imaged using a LI-COR Odyssey CLx (LI-COR Inc) and Image Studio Lite software (LI-COR Inc.). Analysis of colony number and colony size were performed using ImageJ software (NIH).

2D Colony Formation Assay.

1,000 cells were plated on 10cM dishes in full media (10% FBS in DMEM). After 7 days cells derived from KP and KPSik1 GEMMs were washed with PBS, fixed for 10 mins in 10% formalin (EMD Millipore R04586–82) at room temperature, and stained for 20 mins with 0.25% crystal violet (Sigma C3886). Plates were washed, imaged, and analysis of colony number and colony size were performed using ImageJ software.

Survival/Proliferation Assays

Cell survival under detachment conditions (anoikis resistance): 500,000 A549 cells were plated on solidified 1% noble agar-coated P60 plates in full growth media to allow for growth in detached conditions. After 5 days, cells were collected, briefly incubated with TrypLE to produce single cell suspensions and transferred to 24 well plates for proliferation/survival analysis using the CyQuant Direct Cell Proliferation Assay according to the manufacturer's protocol (Invitrogen C35011). Briefly, cells were incubated in staining buffer for 1hr at 37 degrees and analyzed on a Infinite M1000 Pro plate reader (Tecan). For quantification, values from LKB1 add-back and AMPKR knockout cells were divided by values from control A549 cells and expressed as percentage of control.

Adherent cells: 5,000 A549, KP or KPSik1 cells were plated in triplicate in 96 well plates and analyzed using CyQuant assay at time zero, 24hr, 48hr and 72hr timepoints to infer relative cell proliferation. Values for each cell line are divided by values collected at time zero and are expressed as percent growth.

IL-6 quantification

To assess IL-6 secretion by tumor cells, 0.5M A549 or KP CRISPR-modified cells were plated in duplicate in 6 well plates containing 1.5ml of full media (10% FBS in DMEM). Supernatants were harvested after 48 hours and flash frozen in liquid nitrogen before use. Human and mouse IL-6 ELISA assays were performed per manufacturer's instructions (BD). Briefly, plates were prepared overnight with IL-6 antibody and 100ul of each sample was loaded in duplicate in 96 well plates. As needed, supernatants were diluted and reassessed to stay within the standard range of detection of the assay.

CRISPR/Cas9 Studies

Small Guide RNAs (sgRNAs) targeting human or mouse AMPKRs were selected using the optimized CRISPR design tool (http://crispr.mit.edu). Guides with high targeting scores and low probability of off-target effects were chosen, targeting the 1st or 2nd coding exon, or otherwise the first most common downstream exon for transcripts reported to produce multiple isoforms from searches of Uniprot or Ensembl databases. At least two independent sgRNA sequences were selected for each gene. Oligonucleotides for sgRNAs were synthesized by IDT, annealed in vitro and subcloned into either BbsI-digested pSpCas9(BB)-2A-Puro (pX459) vector (Addgene No. 48139), and BsmbI-digested lentiCRISPRv.2-puro (Addgene 52961) lentiCas9-Blast (Addgene 52962), or pSECC (Addgene No 60820). Validation of guide specificity was assessed by Western blot of low-passage A549 human or 634T murine cells transfected with control non-targeting guides, sgTom, or sgLacZ, or sgAMPKR guides with pX459 followed by transient selection (48hrs) with 2ug/ml puromycin, or stable integration of pLentiCRISPRv.2 or lentiCas9-Blast counterparts by lentiviral transduction with 0.45um-filtered viral supernatant supplemented with polybrene followed by selection with 2ug/ml puromycin or 10ug/ml blasticidin. 2-D proliferation assays, anoikis resistance assays and colony growth in soft agar assays were performed with cells stably expressing sgRNAs from pLentiCRISPRv.2-puro and lentiCas9-Blast. pSECC lentiviral vectors harboring identical mouse sgRNAs were utilized for large-scale viral production for *in vivo* delivery. Oligonucleotide sequences are listed in Supplemental Table S1.

Lentiviral production and Titering

Lentiviruses made from pLentiCRISPRv.2, pSECC and Lenti pGK-Cre (latter vector was a gift from Tyler Jacks) were produced by co-transfection of the lentiviral backbone constructs and packaging plasmids pSPAX2 (Addgene 12260) and pMD2.G (Addgene 12259). For low-scale preps, Lipofectamine 2000 (Thermo Fisher Scientific) was used as a transfection reagent at a ratio of 3:1 lipofectamine/DNA. For large-scale preps, the transfection reagent was 1ug/ul PEI, pH4.5 (Polysciences #23966–2) at a ratio of 4:1 PEI/DNA). Viral supernatant was collected 48 and 72 hrs post-transfection, concentrated by

ultracentrifugation at 20,000 RPM for 120 minutes and resuspended in small volumes of 1X HBSS prior to aliquoting, flash freezing and storage at −80°C. Most large-scale viral preps were made in-house and were supplemented as needed with custom orders prepared by the Salk Institute GT3 Viral Vector Core or the University of Iowa Viral Vector Core. Titering: Lentiviral preps for mouse experiments (pSECC and PGK-Cre) were functionally titered by transduction of a reporter line (293-LSL-GFP), which turns on expression of GFP upon Cre-mediated recombination and allows quantitation of functional titers derived from the percent of GFP-positive cells obtained by flow cytometry. The formula used to calculate Transforming Units/ml (TU/ml) was TU/ml = (percent GFP+ cells X number of cells seeded) / (volume of virus used X dilution fold factor. Briefly, 80,000 293-LSL-GFP cells were plated on 24-well plates on day 0 and transduced on day 1 in duplicate across four 2-fold serial dilutions of virus supernatant. After 48hrs, cells were collected, fixed, and analyzed by flow cytometry to calculate % GFP positivity with an LSRII (BD Biosciences). TU/ml titers for each virus were derived from the average TU/ml across the dilution series, assayed two independent times in duplicate wells for each virus. All viruses used together in a given experiment were titered in a batch, and were subsequently normalized to deliver equal number of TU/mouse.

Mouse Studies

GEMM and CRISPR models: All procedures using animals were approved by the Salk Institute Institutional Animal Care and Use Committee (IACUC). All mice were maintained on the FVB/n background. **Kras** (*Kras*$^{LSLG12D/+;}$ *R26*$^{LSL;luc/luc}$); **KL** (*Kras*$^{LSLG12D/+;}$ *Lkb1*$^{fl/fl}$;*R26*$^{LSL;luc/luc}$), **KP** (*Kras*$^{LSLG12D/+;}$ *p53*$^{fl/fl}$;*R26*$^{LSL;luc/luc}$), and **KPL** (*Kras*$^{LSLG12D/+;}$ *Lkb1*$^{fl/fl}$;*p53*$^{fl/fl}$;*R26*$^{LSL;luc/luc}$) mice in FVB/n have been previously described[7] [22]*Sik1*$^{fl/fl}$ and *Sik2*$^{fl/fl}$ conditional floxed mice have also recently been described [32, 33]. In this study, *Sik2*$^{fl/fl}$ was crossed into the FVB/n K background for 8 generations and *Sik1*$^{fl/fl}$ into the FVB/n K and KP background for 4 generations before generating experimental mice. All experiments used a mixture of female and male mice. Experimental endpoint was defined across experiments as the time point at which the experimental cohorts of K+sgLKB1, KL or KPL mice reached tumor burden of 10^9 mean photon flux. Experiments were stopped at that time, and all mice in that experiment were collected at that point. All animals at experimental endpoint were included for analysis of lung tumor burden and tumor size analysis. No animals were excluded from longitudinal BLI measurements and graphs. Because of the different kinetics of tumor growth inherent in K and KP animals, experiments with K and KP animals were considered independent of each other, and thus specific amounts of virus were administered to each set of K and KP animals. Viruses were delivered by intratracheal intubation, according by the protocol of DuPage [53]. Amounts of virus delivered per mouse are as follows: 75K TU/ml (transforming units/ml) of pSECC for Kras animals, 50K TU/ml pSECC for KP animals. 2×10^6 TU/ml PGK-Cre to Kras animals, 4×10^5 for KP animals. 4×10^5 for KP animals. Intravenous lung tumor studies: 8 week old female SCID/Beige mice (PrkdcscidLystbg-J/Crl:Fox Chase, cat #250) were injected with 1 × 106 luciferase expressing A549 cells into the lateral tail vein. All mice were imaged via bioluminescence imaging (BLI) 30 mins after i.v injection. BLI was performed once per week for a period of 52 days.

BLI imaging

Bioluminescent imaging was performed biweekly for all cohorts, with the exception of the floxed KP/KPSik1/KPL cohort, which was imaged weekly. All imaging was done using an IVIS Spectrum (Caliper Life Sciences). Mice were injected intraperitoneally with 150mg/kg D-luciferin (Caliper Life Science, Hopkinton MA), anesthetized with isoflurane and imaged both ventrally and dorsally 10 minutes post luciferin injection. The total lung photon flux for each animal is calculated by the combination of ventral and dorsal photon flux calculated within a region of interest (ROI) encompassing the thorax.

Immunohistochemistry and image analysis

Lungs from mice were collected at each experimental endpoint as noted in the Figures, and were fixed in formalin for 16hrs, transferred to 70% ethanol and paraffin-embedded (FFPE) at the Salk Institute Histology Core or Pacific Pathology (San Diego, CA). 5um sections were prepared and stained with hematoxylin and eosin for tumor burden quantitation. For BrdU IHC, slides were deparaffinized and rehydrated, and antigen retrieval was performed for 30 minutes at high heat in citrate buffer. Endogenous peroxidase activity was quenched with hydrogen peroxide. Slides were blocked with 5% goat serum, incubated overnight with primary anti-BrdU antibody diluted in blocking buffer, and secondary antibody incubation was carried out according to the manufacturer's instructions (ImmPress HRP Reagent kit, Vector Labs MP-7444). Staining was visualized with ImmPACT DAB peroxidase substrate (Vector Labs, SK-4105), and further counterstained with hematoxylin, dehydrated through ethanol and xylenes, and mounted with Cytoseal 60 (Thermo Scientific). H&E- and immunostained slides were scanned using a Perkin Elmer Slide Scanner (Panoramic MIDI Digital Side Scanner) for further downstream analysis using Inform v2.1 image analysis software (Cambridge Research and Instrumentation).

Lung tumor burden

Total lung tumor burden was quantitated from H&E sections using Inform v2.1 image analysis software (Cambridge Research and Instrumentation) in a non-biased manner. In brief, the Trainable Tissue Segmentation method was trained to identify tumor, normal lung, vessel and space. This program was then applied to all H&E images, and each of the resulting mapped images was then screened to verify that accurate tissue segmentation had occurred. The quantitation data from this analysis was then used to calculate the percentage of tumor area as normalized to total lung area (tumor area + normal lung area).

Tumor Size Quantitation

Quantitation of each individual tumor was measured from H&E sections using morphometric analysis in Panoramic viewer software (Perkin Elmer), which calculates the size of each identified tumor by area in squared microns. The area of all tumors found in 5 lobes of each mouse was exported and compiled to plot every tumor per mouse. The data were plotted for each mouse on an x axis and tumor size on the y-axis.

BrdU positivity analysis

For each tumor analyzed, image preparation and tissue and cell segmentation were performed by Inform to calculate the ratio of diaminobenzidine (DAB) positive nuclei out of the total number of hematoxilin-stained nuclei per tumor in order to derive a percent BrdU positive score for each tumor. All individually cropped tumor images were analyzed simultaneously as a batch and verified for accuracy in a blinded manner to exclude extreme outlier images from final analysis.

Immunoblots

Protein lysates from cells were isolated in cold 1% NP-40 RIPA buffer supplemented with protease inhibitors (cOmplete, Roche) and phosphatase inhibitors (PhosStop, Roche). Lysates were normalized using a BCA protein assay kit (Pierce) and resolved on 8% SDS-PAGE gels.

Antibodies

For western blotting, antibodies from Cell Signaling Technologies (Denvers, MA USA) were used diluted at 1:1000 unless otherwise noted: pLKB1 (#3047), Total AMPKα (#2532), P-AMPK(T172) (#2535), P-ACCS79 (#3661), pRAPTOR (S792) (#2083), BRSK1 (#5935, 1:500), BRSK2 (#5460), MARK2 (#9118), MARK3 (#9311), MARK4 (#4834, 1:500), pMARK activation loop (#4836), NUAK1 (#4458), SIK2 (#6919), GAPDH (#5174, 1:10,000), NR4A1 (#3960), pHDAC4/5/7(S246) (#3443), STAT3 (#9139) (STAT1 (#14994S), pSTAT1-Y701 (#9167) pSIK family T-loop antibody: (Abcam 199474, 1:000), SIK1: rabbit polyclonal 1–111 (kind gift from Rebecca Berdeaux). SIK3 (human) (Novus, NBP2–47278), SIK3 (mouse) (Bethyl A302–455A), NUAK2 (Novus NBP1–81880, 1:1000), SNRK (ab173538, 1:500), CRTC3 (ab91654, 1:1000), CRTC2 (Calbiochem ST1099, 1:10,000), pCRTC2: kind gift from Marc Montminy. FLAG-M2-affinity gel (Sigma A2220). For IHC, BrdU (Abcam #6326, 1:200), Ly-6G (Biolegend, clone 1A8, 1:200).

SIK1 PCR

To validate loss of SIK1 in lung tumors, DNA was isolated from flash frozen tumor tissue derived from control K+sgTom, KSik1, and KSik1+sgSik3 tumors using the Quick-RNA Miniprep kit (Zymo Research) and PCR was performed with primers to amplify the recombined SIK1 allele or primers to amplify the floxed allele as described in Nixon et al [32].

mRNA preparation and qPCR.

mRNA from snap-frozen tumor samples was prepared using the Quick-RNA Miniprep kit (Zymo Research), including DNase treatment. cDNA was synthesized from 2 μg of RNA using SuperScript III (Life Technologies), and qPCR was carried out with diluted cDNA, appropriate primers, and SYBR Green PCR master mix (ThermoFisher Scientific) using a C1000 Thermal Cycler (BioRad). Relative mRNA levels were calculated using the 2− Ct method, using actin as an internal control.

mRNA-seq

Tumor RNA was isolated using the Quick-RNA MiniPrep kit (Zymo Research), including a DNase treatment. RNA integrity (RIN) numbers were determined using the Agilent TapeStation prior to library preparation. mRNA-seq libraries were prepared using the TruSeq RNA library preparation kit (version 2), according to the manufacturer's instructions (Illumina). Libraries were quantified, pooled, and sequenced by single-end 50 base pairs using the Illumina HiSeq 2500 platform at the Salk Next-Generation Sequencing Core. Raw sequencing data were demultiplexed and converted into FASTQ files using CASAVA (version 1.8.2). Libraries were sequenced at an average depth of 80 million reads per sample.

Deep sequencing and bioinformatics analysis of Cas9 target loci

Tumor DNA was obtained by laser-capture-microdissection at the Biophotonics core at the Salk Institute. DNA was isolated from lung histology sections to represent all sgRNA guides used in this study and was prepared with the Arcturus PicoPure DNA extraction Kit (ABI), with subsequent cleanup with AmpPure beads (Agilent). For each targeted gene, a 300bp amplicon centered around the PAM site was amplified using NEB Next 2X master mix. Sequencing libraries were prepared from 50–80ng of tumor PCR product and barcoded with custom index R2 primers (kind gift from Patrick Hsu). Individual libraries were quantitated after electrophoresis with analytical quantitative ladder, and relative molar amounts of barcoded amplicons were pooled, cleaned up with AmpPure beads and gel purified 2X. Final pooled libraries were characterized for size by TapeStation, quantitated by qPCR using KAPA Library quantification kit, and were sequenced on an Illumina MiSeq machine with 300bp end-paired reads. MiSeq reads were filtered by requiring an average Phred quality (Q score) of at least 30, as well as perfect sequence matches to barcodes. Data was demultiplexed with a custom script and pair-end stitching was done with Pear. The python program CRIS.py v2 was applied to stitched data to assess endonuclease activity. CRIS.py output was used to quantify the edit rate, frame shift rate, and average indel size of all clones.

Bioinformatic analysis for RNAseq

Sequenced reads were quality-tested using the online FASTQC tool (http://www.bioinformatics.babraham.ac.uk/projects/fastqc) and aligned to the mouse mm10 genome using the STAR aligner version 2.4.0k. Raw gene expression was quantified across all annotated exons using HOMER [54], and differential gene expression was carried out using the edgeR package version 3.6.8 using duplicates to compute within-group dispersion and correcting for batch effects [55]. Differentially expressed genes were defined as having a false discovery rate (FDR) <0.05 and a log2 fold change >0.59. GSEA was carried out with the GenePattern interface, https://genepattern.broadinstitute.org) using preranked lists generated from FDR values, setting gene set permutations to 1000 and using the Hallmark collection in MSigDB version5.0. Clustering was performed with Gene Cluster 3.0 and visualized by heat maps using Java TreeView (version 1.1.6r4). Area-proportional Venn diagrams were plotted using BioVenn [56]. Metascape: http://metascape.org. Enrichr: http://

amp.pharm.mssm.edu/Enrichr. Homer motif enrichment analysis: http://homer.ucsd.edu/homer/motif/.

Statistical analyses.

Statistical analyses are described in each figure were all performed using Graph Pad Prism 7.

Supplementary Material

Refer to Web version on PubMed Central for supplementary material.

ACKNOWLEDGEMENTS

This study was supported by grants to R.J.S. from the National Institutes of Health (R35CA220538, P01CA120964), the Samuel Waxman Cancer Research Foundation, and The Leona M. and Harry B. Helmsley Charitable Trust grant #2012-PG- MED002. R.U.S. was supported by a postdoctoral fellowship from the American Cancer Society (ACS#124183-PF-13-023-01-CSM). L.J.E. is supported by a postdoctoral fellowship from the American Cancer Society (PF-15-037-01-DMC). S.N.B was supported by training grant 5T32CA009370 to the Salk Institute Cancer Center and 5F32CA206400. The Salk CCSG P30 CA014195 and Helmsley Charitable Trust supported the Functional Genomics Core and the Bioinformatics Core. We thank Thales Papagiannakopoulos (NYU) and Francisco Sánchez-Rivera (MSKCC) for advice regarding pSECC viral preparation. We additionally are grateful to Nasun Ha and the Salk Next-Generation Sequencing Core for helpful discussions, Marc Montminy, Ezra Wiater and Patrick Hsu for assistance and discussions regarding Miseq, Jill Meisenhelder and Xavier Miralles Fusté for helpful advice with in vitro kinase reactions, and Jeanine Van Nostrand for help with intratracheal intubations. We thank Matthew Chun for help with transcription analysis in human NSCLC cells and Daniel Garcia for help with graphic design. We thank Chris Murray and Monte Winslow of Stanford for helpful discussions, and members of the Shaw lab for feedback and advice.

References

1. Hemminki A, et al., A serine/threonine kinase gene defective in Peutz-Jeghers syndrome. Nature, 1998 391(6663): p. 184–7. [PubMed: 9428765]
2. Ding L, et al., Somatic mutations affect key pathways in lung adenocarcinoma. Nature, 2008 455(7216): p. 1069–75. [PubMed: 18948947]
3. Sanchez-Cespedes M, et al., Inactivation of LKB1/STK11 is a common event in adenocarcinomas of the lung. Cancer Res, 2002 62(13): p. 3659–62. [PubMed: 12097271]
4. Chen Z, et al., A murine lung cancer co-clinical trial identifies genetic modifiers of therapeutic response. Nature, 2012 483(7391): p. 613–7. [PubMed: 22425996]
5. Han X, et al., Transdifferentiation of lung adenocarcinoma in mice with Lkb1 deficiency to squamous cell carcinoma. Nat Commun, 2014 5: p. 3261. [PubMed: 24531128]
6. Ji H, et al., LKB1 modulates lung cancer differentiation and metastasis. Nature, 2007 448(7155): p. 807–10. [PubMed: 17676035]
7. Shackelford DB, et al., LKB1 inactivation dictates therapeutic response of non-small cell lung cancer to the metabolism drug phenformin. Cancer Cell, 2013 23(2): p. 143–58. [PubMed: 23352126]
8. Svensson RU, et al., Inhibition of acetyl-CoA carboxylase suppresses fatty acid synthesis and tumor growth of non-small-cell lung cancer in preclinical models. Nat Med, 2016 22(10): p. 1108–1119. [PubMed: 27643638]
9. Zhang H, et al., Lkb1 inactivation drives lung cancer lineage switching governed by Polycomb Repressive Complex 2. Nat Commun, 2017 8: p. 14922. [PubMed: 28387316]
10. Skoulidis F, et al., Co-occurring genomic alterations define major subsets of KRAS-mutant lung adenocarcinoma with distinct biology, immune profiles, and therapeutic vulnerabilities. Cancer Discov, 2015 5(8): p. 860–77. [PubMed: 26069186]

11. Koyama S, et al., STK11/LKB1 Deficiency Promotes Neutrophil Recruitment and Proinflammatory Cytokine Production to Suppress T-cell Activity in the Lung Tumor Microenvironment. Cancer Res, 2016 76(5): p. 999–1008. [PubMed: 26833127]
12. Biton J, et al., TP53, STK11, and EGFR Mutations Predict Tumor Immune Profile and the Response to Anti-PD-1 in Lung Adenocarcinoma. Clin Cancer Res, 2018.
13. Rizvi H, et al., Molecular Determinants of Response to Anti-Programmed Cell Death (PD)-1 and Anti-Programmed Death-Ligand 1 (PD-L1) Blockade in Patients With Non-Small-Cell Lung Cancer Profiled With Targeted Next-Generation Sequencing. J Clin Oncol, 2018 36(7): p. 633–641. [PubMed: 29337640]
14. Skoulidis F, et al., STK11/LKB1 Mutations and PD-1 Inhibitor Resistance in KRAS-Mutant Lung Adenocarcinoma. Cancer Discov, 2018 8(7): p. 822–835. [PubMed: 29773717]
15. Lizcano JM, et al., LKB1 is a master kinase that activates 13 kinases of the AMPK subfamily, including MARK/PAR-1. EMBO J, 2004 23(4): p. 833–43. [PubMed: 14976552]
16. Shackelford DB and Shaw RJ, The LKB1-AMPK pathway: metabolism and growth control in tumour suppression. Nat Rev Cancer, 2009 9(8): p. 563–75. [PubMed: 19629071]
17. Faubert B, et al., AMPK is a negative regulator of the Warburg effect and suppresses tumor growth in vivo. Cell Metab, 2013 17(1): p. 113–24. [PubMed: 23274086]
18. Houde VP, et al., AMPK beta1 reduces tumor progression and improves survival in p53 null mice. Mol Oncol, 2017 11(9): p. 1143–1155. [PubMed: 28544264]
19. Chan LN, et al., Metabolic gatekeeper function of B-lymphoid transcription factors. Nature, 2017 542(7642): p. 479–483. [PubMed: 28192788]
20. Kishton RJ, et al., AMPK Is Essential to Balance Glycolysis and Mitochondrial Metabolism to Control T-ALL Cell Stress and Survival. Cell Metab, 2016 23(4): p. 649–62. [PubMed: 27076078]
21. Saito Y, et al., AMPK Protects Leukemia-Initiating Cells in Myeloid Leukemias from Metabolic Stress in the Bone Marrow. Cell Stem Cell, 2015 17(5): p. 585–96. [PubMed: 26440282]
22. Eichner LJ, et al., Genetic Analysis Reveals AMPK Is Required to Support Tumor Growth in Murine Kras-Dependent Lung Cancer Models. Cell Metab, 2019 29(2): p. 285–302 e7. [PubMed: 30415923]
23. Cheng H, et al., SIK1 couples LKB1 to p53-dependent anoikis and suppresses metastasis. Sci Signal, 2009 2(80): p. ra35. [PubMed: 19622832]
24. Ahmed AA, et al., SIK2 is a centrosome kinase required for bipolar mitotic spindle formation that provides a potential target for therapy in ovarian cancer. Cancer Cell, 2010 18(2): p. 109–21. [PubMed: 20708153]
25. Tarumoto Y, et al., LKB1, Salt-Inducible Kinases, and MEF2C Are Linked Dependencies in Acute Myeloid Leukemia. Mol Cell, 2018 69(6): p. 1017–1027 e6. [PubMed: 29526696]
26. Patra KC, et al., Mutant GNAS drives pancreatic tumourigenesis by inducing PKA-mediated SIK suppression and reprogramming lipid metabolism. Nat Cell Biol, 2018 20(7): p. 811–822. [PubMed: 29941929]
27. Itoh Y, et al., Salt-inducible Kinase 3 Signaling Is Important for the Gluconeogenic Programs in Mouse Hepatocytes. J Biol Chem, 2015 290(29): p. 17879–93. [PubMed: 26048985]
28. Patel K, et al., The LKB1-salt-inducible kinase pathway functions as a key gluconeogenic suppressor in the liver. Nat Commun, 2014 5: p. 4535. [PubMed: 25088745]
29. Chen Z, et al., Non-small-cell lung cancers: a heterogeneous set of diseases. Nat Rev Cancer, 2014 14(8): p. 535–46. [PubMed: 25056707]
30. Sanchez-Rivera FJ, et al., Rapid modelling of cooperating genetic events in cancer through somatic genome editing. Nature, 2014 516(7531): p. 428–31. [PubMed: 25337879]
31. Platt RJ, et al., CRISPR-Cas9 knockin mice for genome editing and cancer modeling. Cell, 2014 159(2): p. 440–55. [PubMed: 25263330]
32. Nixon M, et al., Skeletal muscle salt inducible kinase 1 promotes insulin resistance in obesity. Mol Metab, 2016 5(1): p. 34–46. [PubMed: 26844205]
33. Sakamaki J, et al., Role of the SIK2-p35-PJA2 complex in pancreatic beta-cell functional compensation. Nat Cell Biol, 2014 16(3): p. 234–44. [PubMed: 24561619]

34. Luo Y and Zheng SG, Hall of Fame among Pro-inflammatory Cytokines: Interleukin-6 Gene and Its Transcriptional Regulation Mechanisms. Front Immunol, 2016 7: p. 604. [PubMed: 28066415]
35. Hollstein PE and Shaw RJ, Inflamed T cells and stroma drive gut tumors. Science, 2018 361(6400): p. 332–333. [PubMed: 30049865]
36. Hardie DG, Ross FA, and Hawley SA, AMPK: a nutrient and energy sensor that maintains energy homeostasis. Nat Rev Mol Cell Biol, 2012 13(4): p. 251–62. [PubMed: 22436748]
37. Mukhopadhyay A, et al., Sox2 cooperates with Lkb1 loss in a mouse model of squamous cell lung cancer. Cell Rep, 2014 8(1): p. 40–9. [PubMed: 24953650]
38. Xu C, et al., Loss of Lkb1 and Pten leads to lung squamous cell carcinoma with elevated PD-L1 expression. Cancer Cell, 2014 25(5): p. 590–604. [PubMed: 24794706]
39. Gilbert-Ross M, et al., Targeting adhesion signaling in KRAS, LKB1 mutant lung adenocarcinoma. JCI Insight, 2017 2(5): p. e90487. [PubMed: 28289710]
40. Murray CW, et al., An Lkb1-Sik axis suppresses lung tumor growth and controls differentiation.
41. Berdeaux R, et al., SIK1 is a class II HDAC kinase that promotes survival of skeletal myocytes. Nat Med, 2007 13(5): p. 597–603. [PubMed: 17468767]
42. Henriksson E, et al., SIK2 regulates CRTCs, HDAC4 and glucose uptake in adipocytes. J Cell Sci, 2015 128(3): p. 472–86. [PubMed: 25472719]
43. Park J, et al., SIK2 is critical in the regulation of lipid homeostasis and adipogenesis in vivo. Diabetes, 2014 63(11): p. 3659–73. [PubMed: 24898145]
44. Canettieri G, et al., The coactivator CRTC1 promotes cell proliferation and transformation via AP-1. Proc Natl Acad Sci U S A, 2009 106(5): p. 1445–50. [PubMed: 19164581]
45. Bittinger MA, et al., Activation of cAMP response element-mediated gene expression by regulated nuclear transport of TORC proteins. Curr Biol, 2004 14(23): p. 2156–61. [PubMed: 15589160]
46. Iourgenko V, et al., Identification of a family of cAMP response element-binding protein coactivators by genome-scale functional analysis in mammalian cells. Proc Natl Acad Sci U S A, 2003 100(21): p. 12147–52. [PubMed: 14506290]
47. Chen Z, et al., Aberrantly activated AREG-EGFR signaling is required for the growth and survival of CRTC1-MAML2 fusion-positive mucoepidermoid carcinoma cells. Oncogene, 2014 33(29): p. 3869–77. [PubMed: 23975434]
48. Feng Y, et al., The CRTC1-NEDD9 signaling axis mediates lung cancer progression caused by LKB1 loss. Cancer Res, 2012 72(24): p. 6502–11. [PubMed: 23074285]
49. Carretero J, et al., Integrative genomic and proteomic analyses identify targets for Lkb1-deficient metastatic lung tumors. Cancer Cell, 2010 17(6): p. 547–59. [PubMed: 20541700]
50. Ollila S, et al., Stromal Lkb1 deficiency leads to gastrointestinal tumorigenesis involving the IL-11-JAK/STAT3 pathway. J Clin Invest, 2018 128(1): p. 402–414. [PubMed: 29202476]
51. Poffenberger MC, et al., LKB1 deficiency in T cells promotes the development of gastrointestinal polyposis. Science, 2018 361(6400): p. 406–411. [PubMed: 30049881]
52. Yong Kim S, et al., Salt-inducible kinases 1 and 3 negatively regulate Toll-like receptor 4-mediated signal. Mol Endocrinol, 2013 27(11): p. 1958–68. [PubMed: 24061540]
53. DuPage M, Dooley AL, and Jacks T, Conditional mouse lung cancer models using adenoviral or lentiviral delivery of Cre recombinase. Nat Protoc, 2009 4(7): p. 1064–72. [PubMed: 19561589]
54. Heinz S, et al., Simple combinations of lineage-determining transcription factors prime cis-regulatory elements required for macrophage and B cell identities. Mol Cell, 2010 38(4): p. 576–89. [PubMed: 20513432]
55. Robinson MD, McCarthy DJ, and Smyth GK, edgeR: a Bioconductor package for differential expression analysis of digital gene expression data. Bioinformatics, 2010 26(1): p. 139–40. [PubMed: 19910308]
56. Hulsen T, de Vlieg J, and Alkema W, BioVenn - a web application for the comparison and visualization of biological lists using area-proportional Venn diagrams. BMC Genomics, 2008 9: p. 488. [PubMed: 18925949]

Significance

The tumor suppressor LKB1/STK11 encodes a serine/threonine kinase frequently inactivated in NSCLC. LKB1 activates 14 downstream kinases in the AMPK family controlling growth and metabolism, though which kinases are critical for LKB1 tumor suppressor function has remained an enigma. Here we unexpectedly found that two understudied kinases, SIK1 and SIK3, are critical targets in lung cancer.

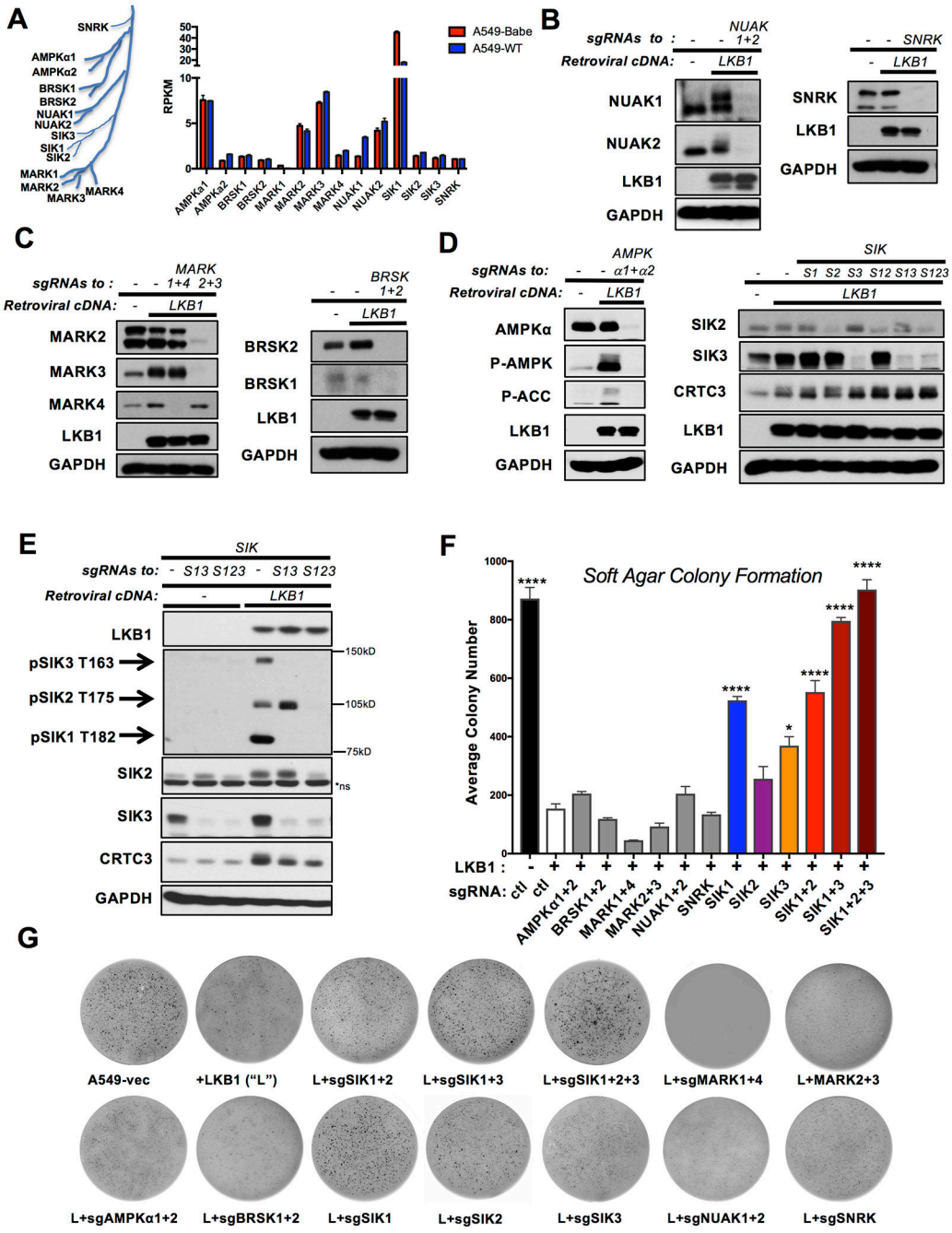

Figure 1. A lentiviral CRISPR-based screen targeting the AMPK-Related (AMPKR) kinase family in human NSCLC cells reveals the SIK subfamily mediates tumor suppressive phenotypes of LKB1.

(A) Left: schematic of the AMPK-Related (AMPKR) kinase family tree branch. Right: RPKM (Reads per kilobase million) plot showing the relative mRNA expression of the AMPKR kinase family in human A549 (LKB1-null) and LBK1 WT-reconstituted cells. (B-D) Western blots on lysates from A549-LKB1 WT cells treated with lentiviral sgRNAs targeting the AMPKR family. Control sgRNA-treated A549 (LKB1-null) and A549-LKB1 WT cells also shown.

(B) Western blots of lysates from A549-LKB1 WT cells targeted to co-delete NUAK1+NUAK2 (left), and SNRK (right).
(C) Western blot of lysates from A549-LKB1 WT cells targeted to co-delete MARK1+MARK4, MARK2+MARK3, and BRSK1+BRSK2.
(D) Left: Western blots of lysates from A549-LKB1 WT cells targeted to delete AMPK catalytic subunits α1/2. Right: Western blots of lysates from A549-LKB1 WT cells targeted to delete the SIK subfamily, either with individual guides against SIK1, SIK2, and SIK3, or using combinations of guides to co-delete SIK1+SIK2, SIK1+SIK3, and SIK1+2+3.
(E) Western blots on lysates from A549-pBabe and A549-LKB1 WT cells targeted to co-delete SIK1 + SIK3 or SIK1+SIK2+SIK3. SIK kinases are only phosphorylated in the presence of LKB1 and cell lines targeted for SIK deletion show loss of phosphorylation only on the targeted SIK proteins, validating deletion in these lines.
(F) Soft agar colony formation of AMPKR-deficient cells. Average colony number after 3 weeks of growth in soft agar is shown. Assays were done two times in triplicate wells and the values represent the average of independently generated cell lines for a given AMPKR as described in Figure S1E. *P<0.05, **** P<0.0001 by ANOVA and post hoc student's t-test.
(G) Representative images of soft agar colony growth of A549 (LKB1-null) cells, A549 LKB1-WT ("L") cells and AMPKR-deficient A549 LKB1-WT cells.

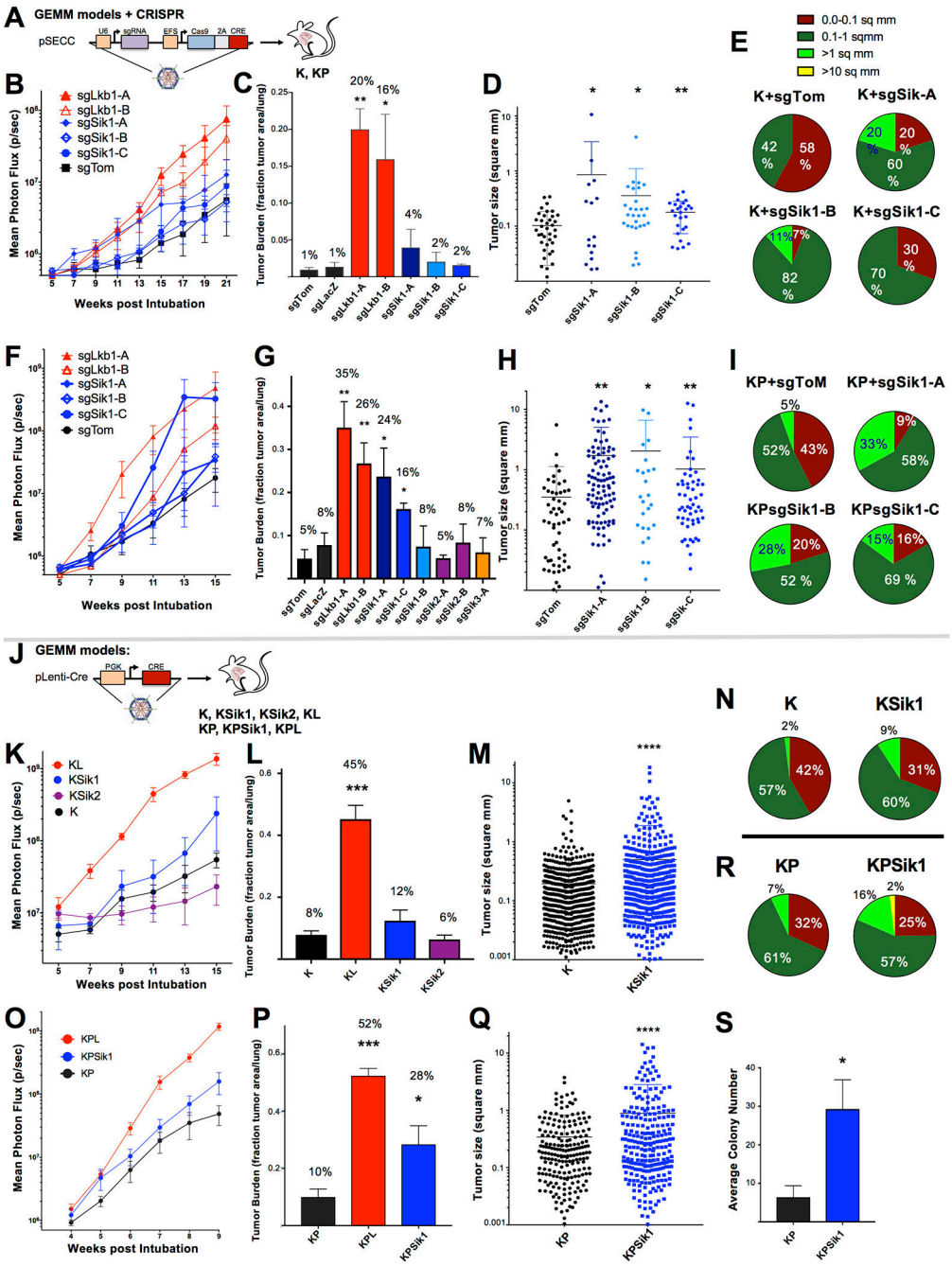

Figure 2. CRISPR-based and GEMM-based mouse models of SIK family kinase inactivation in Kras-driven NSCLC demonstrate acceleration of tumor growth upon SIK1 loss.

(A) Schematic of the experimental design using pSECC lentivirus to deliver Cre-recombinase, Cas9 and a sgRNA of choice as a single payload to the lungs of KrasG12D-mice (K) and Kras-p53 floxed mice (KP) after intratracheal virus delivery.

(B-E) Analysis of inactivating Sik1 or Lkb1 with pSECC-sgRNA viruses in the lungs of K mice.

(B) Longitudinal bioluminescent imaging (BLI) data from induced tumors in K mice treated with pSECC control (sgTom, N=4 or sgLacZ in Figure 2C, N=3), sgLkb1 (N=10), and three

independent sgSik1 viruses (N=11). Average bioluminescence (photon flux) at each imaging time point is shown for each cohort. The last point shown indicates study endpoint.
(C) Quantitation of tumor burden. Tumor area was calculated as a percent of total lung area from H&E-stained sections for each mouse. The average tumor burden for each cohort is shown as a fraction of tumor area/total lung.
(D) Quantitation of individual tumor size in lungs of K mice treated with pSECC-control (sgTom) and pSECC-sgSik1-viruses. The area of individual tumors was quantitated in mm^2 from H&E sections for each mouse and are shown in a dot-plot per cohort for each sgRNA guide. Each dot represents a single tumor, with a bar denoting the average tumor size per cohort.
(E) Distribution in tumor size observed in pSECC-control and pSECC-sgSik1-treated mice. Individual tumors from all mice in each cohort were binned by size and are shown as a percent for each size bin in a pie chart.
(F-I) Analysis of inactivating the SIK kinase family or LKB1 with pSECC-sgRNA viruses in the lungs of KP mice.
(F) Longitudinal BLI data from KP mice treated with control pSECC virus or pSECC viruses harboring sgRNA guides to target mouse LKB1 (N=6), SIK1 (N=10), SIK2 (N=9) and SIK3 (N=7). Average bioluminescence (photon flux) at each imaging time point is shown for each cohort. The last point shown indicates study endpoint.
(G) Tumor burden analysis for all pSECC-treated cohorts of KP mice. Tumor area was calculated as a percentage of total lung area. The average tumor burden for each cohort treated with individual sgRNA guides is shown as a fraction of tumor area/total lung.
(H) Quantitation of individual tumor size (area in mm^2) in pSECC control and pSECC-SIK1-treated KP mice. The number of tumors per cohort treated with individual sgRNA guides targeting SIK1 is shown. Each dot represents an individual tumor, with a bar denoting the average tumor size per cohort.
(I) Tumor size distribution in KP mice treated with control and pSECC-SIK1 viruses. Individual tumors were binned by size and are represented as percentages of different size bins shown in a pie chart.
All values in (B-I) are expressed as means ± s.e.m. *P<0.05, ** P<0.01, *** P< 0.001 determined by student's t test.
(J) Schematic of the experimental design using GEMM mice with floxed alleles of *Sik1, Sik2,* and *Stk11* (LKB1) in a conditional K-RasG12D background (KSik1, KSik2, KL), and *Sik1* and *Stk11* in a conditional KP genetic background (KPSik1 and KPL). Genetic conditional activation of Kras and conditional knockout of the listed genes in the lung is generated by Cre-recombinase-mediated IoxP recombination after intratracheal delivery of pGK-CRE-virus.
(K-N) Analysis of tumor growth, endpoint tumor burden, and tumor size distribution in floxed K, KSik1, KSik2 and KL mice.
(K) Longitudinal bioluminescent imaging (BLI) data from induced lung tumors in floxed K (N=13), KSik1 (N=12), KSik2 (N=6), and KL (N=6) mice after PGK-Cre-mediated recombination. Average bioluminescence (photon flux) at each imaging time point is shown for each cohort. The last point shown indicates study endpoint.

(L) Tumor burden analysis of floxed K, KSik1, KSik2 and KL mice. Tumor area was calculated as a percent of total lung area per mouse, and shown as the average fraction of tumor/lung for each cohort.
(M) Quantitation of tumor size (area in mm^2) in lung tumors from floxed K and and KSik1 mice. Each dot represents an individual tumor, with a bar denoting the average tumor size per cohort.
(N) Tumor size distribution in floxed K and KSik1 mice. Individual tumors were binned by size and are represented as percentages of different size bins shown in a pie chart.
(O-R) Analysis of tumor growth, endpoint tumor burden, and tumor size distribution in floxed KP and KPSik1 mice.
(O) Longitudinal bioluminescent imaging (BLI) data from induced lung tumors in floxed KP (N=8), KPSik1 (N=5), and KPL (N=5) mice after PGK-Cre-mediated recombination. Average bioluminescence (photon flux) at each imaging time point is shown for each cohort. The last point shown indicates study endpoint.
(P) Tumor burden analysis of floxed KP, KPSik1 and KPL mice. Tumor area was calculated as a percent of total lung area per mouse, and shown as the average fraction of tumor/lung for each cohort.
(Q) Quantitation of tumor size (area in mm^2) in individual lung tumors from GEMM KP and KPSik1 mice. Each dot represents an individual with a bar denoting the average tumor size per cohort.
(R) Tumor size distribution in GEMM KP and KPSik1 mice. Individual tumors were binned by size and represented as percentages of different size bins shown in a pie chart.
(S) Colony growth in soft agar of mouse tumor-derived KPSik1 and KP cells lines. Data represent the combined average of n=4 independent KP lines and n=3 independent KPSik1 lines from assays performed in triple wells two times. Graph shows average colony number at a threshold to detect large colonies (50-pixel range).
All values in (K-S) are expressed as means ± s.e.m. *P<0.05, ** P<0.01, *** P< 0.001, ****P<0.001 determined by student's t test.

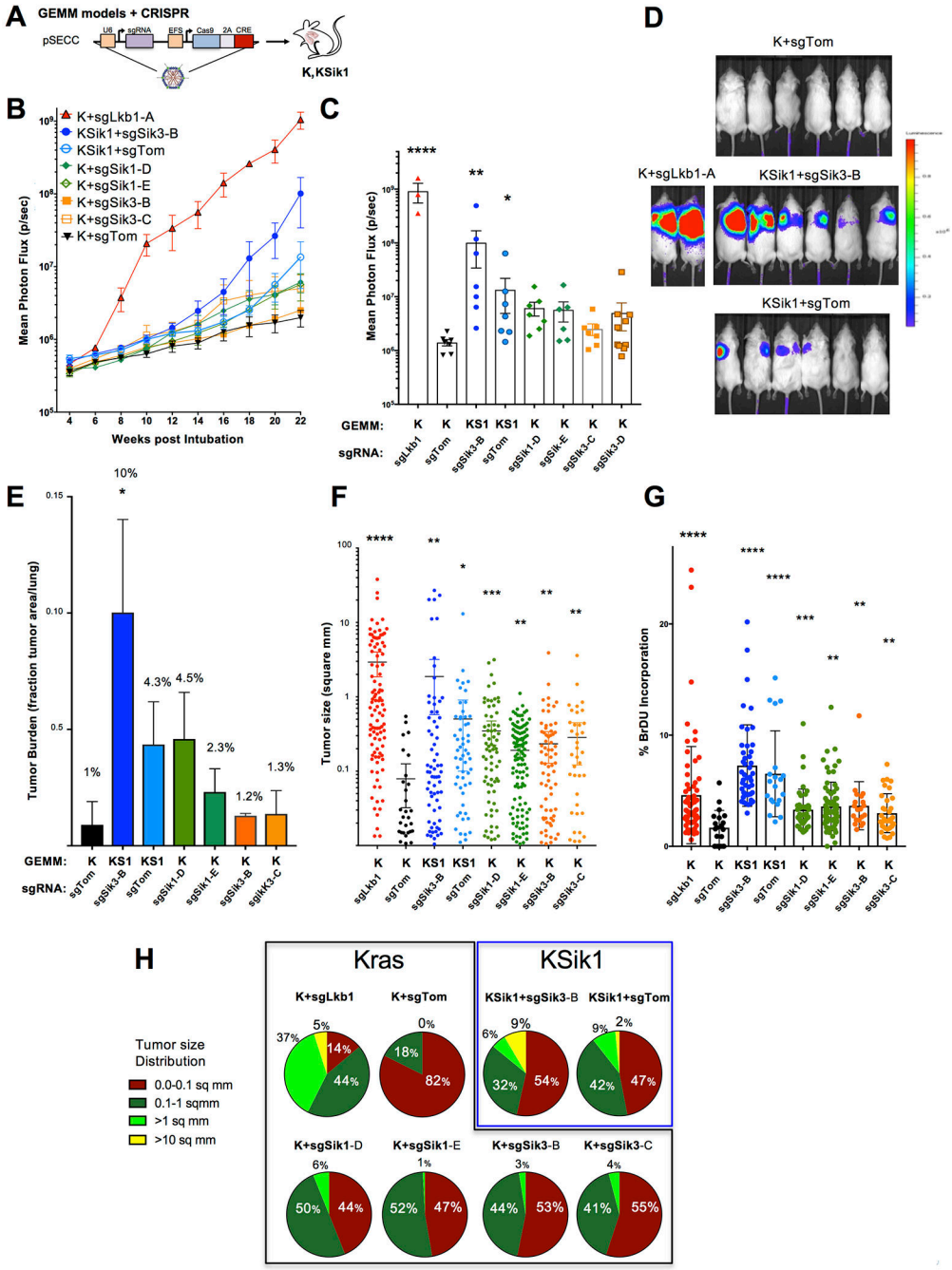

Figure 3. Combined effect on tumor growth by genetic loss of SIK1 with CRISPR-mediated inactivation of SIK3 in a Kras-driven mouse model of NSCLC.

(A) Schematic of the experimental design using pSECC lentivirus to deliver Cre-recombinase, Cas9 and a Sik1 or Sik3 sgRNA as a single payload to the lungs of KrasG12D-mice (K) and Kras-Sik1 floxed mice (KSik1) after intratracheal virus delivery.

(B) Longitudinal bioluminescent imaging (BLI) data from induced lung tumors in GEMM KSik1 mice treated with pSECC control (sgTom) (N=7) or pSECC-sgSik3-B (N=7), and K mice treated with pSECC control (sgTom) (N=7), sgLkb1 (N=3 at study endpoint), or two sgRNA viruses targeting *Sik1*: sgSik1-D, (N=7), sgSik1-E (N=5), or *Sik3*: sgSik3-B (N=9),

sgSik3-C (N=6). Average bioluminescence (photon flux) at each imaging time point is shown for each cohort. The last point shown indicates study endpoint.

(C) BLI data of lung tumors from study endpoint for K and KSik1 mice treated with control sgTom and sgSik guides. Each dot represents the endpoint BLI value for each mouse overlayed on a bar graph denoting the mean for each group.

(D) Overlay of BLI images at study endpoint for K+sgTom, KSik1+sgTom and KSik1+sgSik3 tumor-bearing mice. Shown are N=6 images for mice with the highest amounts of luminescence emitted from lung tumors within each cohort. N=2 images from K +sgLkb1 mice are shown for comparison. Scale bar represents photons/sec/cm^2/sr.

(E) Tumor burden analysis of K+sgTom, KSIK+sgSik3, KSik1+sgTom, and K+sgSik1 and K+sgSik3 mice. Tumor area was calculated as a percent of total lung area per mouse, and shown as the average fraction of tumor/lung for each cohort.

(F) Quantitation of tumor size (area in mm^2) in individual lung tumors from K+sgLkb1, K +sgTom, KSik1+sgSik3, KSik1+sgTom, and K+sgSik1 and K+sgSik3 mice. Each dot represents an individual with a bar denoting the average tumor size per cohort.

(G) BrdU positivity in lung tumors from K+sgLkb1, K+sgTom, KSik1+sgSik3 or sgTom, and K+sgSik1 or sgSik3 mice. Data is displayed as percent BrdU+ cells over total cell number for each tumor. Each dot represents a single tumor within each cohort.

(H) Lung tumor size distribution in Kras (K) and KSik1 mice treated with control or sgSik3 pSECC viruses (KSik1 mice), or control and sgLkb1, sgSik1, and sgSik3 pSECC viruses (K mice). Individual tumors were binned by size and represented as percentages of different size bins shown as a pie chart.

All values in (B-H) are expressed as means ± s.e.m. *P<0.05, ** P<0.01, *** P< 0.001, ****P<0.001 determined by student's t test.

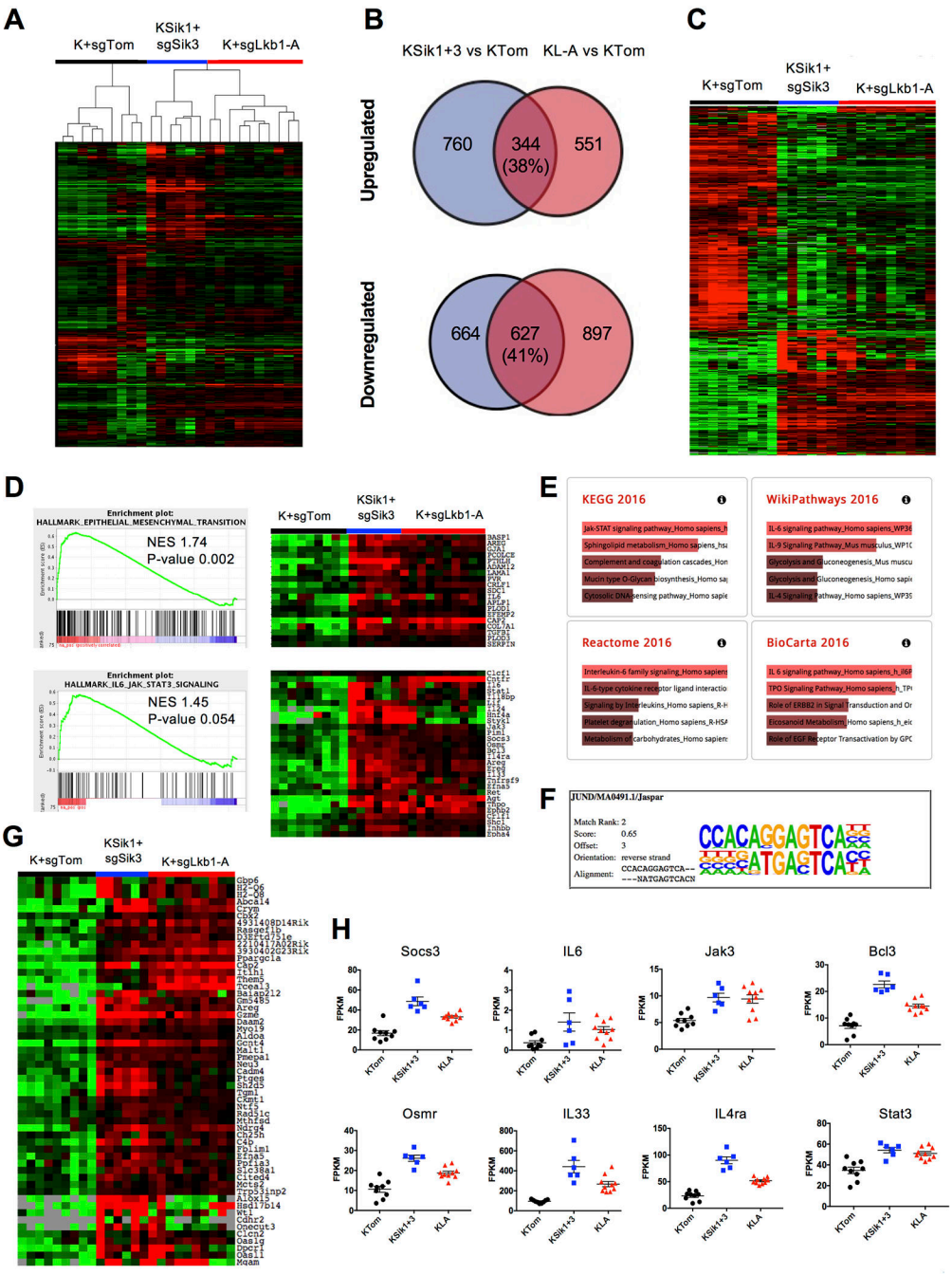

Figure 4. Transcriptional analysis of lung tumors derived from KSik1+sgSik3 and K+sgLkb1 mice reveal a shared core gene signature enriched for upregulation of genes involved in IL6/JAK/STAT and AP-1 signaling pathways.

(A) Transcriptional profile heatmap denoting unbiased clustering of mouse tumors from the following genotypes: K+sgTom (KTom) (n=9), KSik1+sgSik3 (n=6), and KL-A (n=10). Tumor RNA was analyzed by high throughput whole-transcriptome sequencing (RNAseq). Samples clustered by genotype in an unbiased manner.

(B) Differential expression analysis on tumors from (A) (using fold change +/− log2 0.59, FDR <0.05 cut-offs) reveals that 38% of upregulated genes and 41% of downregulated genes

which are LKB1-dependent respond in the same, statistically significant manner to SIK1+SIK3 inactivation.

(C) Cluster of the 971 genes commonly regulated by inactivation of LKB1 or SIK1+3 inactivation identified in Figure 4B.

(D) GSEA plots from KSik1+sgSik3 vs. KTom data queried against the “Hallmark” group of gene sets. Six gene sets were independently identified in both the K+sgLkb1 and KSik1+3 dataset queries. Two of these gene sets, shown in (D), represent biological processes well-established to be induced upon LKB1 deletion. The EMT signature was the top enriched gene set, IL6_JAK_STAT3_Signaling was 8th most enriched gene set. EMT heatmap shows FPKMs for all enriched genes in EMT GSEA plot. IL6 heatmap shows FPKMs for all enriched genes in IL6 GSEA plot combined with Metascape IL6 category genes (Fig S10B).

(E-G) Analysis of the 344 upregulated genes common to both K+sgLkb1 and KSik1+sgSik3.

(E) Enrichr analyses identify IL-6 pathway enrichment only within upregulated genes common to K+sgLkb1 and KSik1+sgSik3.

(F) Homer de novo Motif Enrichment analysis on the upregulated genes common to K +sgLkb1 and KSik1+sgSik3. The only significantly enriched motif (P=1e-12) is shown. The enriched motif corresponds to the JUND/FOS/FOSL1/AP-1/FRA2 motif, JUND motif is pictured.

(G) Heatmap of genes with AP1+CRE elements in the promoter (+/−2kb of TSS).

(H) FPKM plots for genes from the IL-6/JAK/STAT3 signaling pathway. Cytokines (IL6,IL33), receptors (IL4ra), core components (Jak3, Stat3), co-activators (Bcl3, Osmr), and canonical downstream STAT3 transcriptional targets (Socs3) mRNAs were all upregulated in both LKB1-deficient and SIK1+SIK3-deficient tumors.

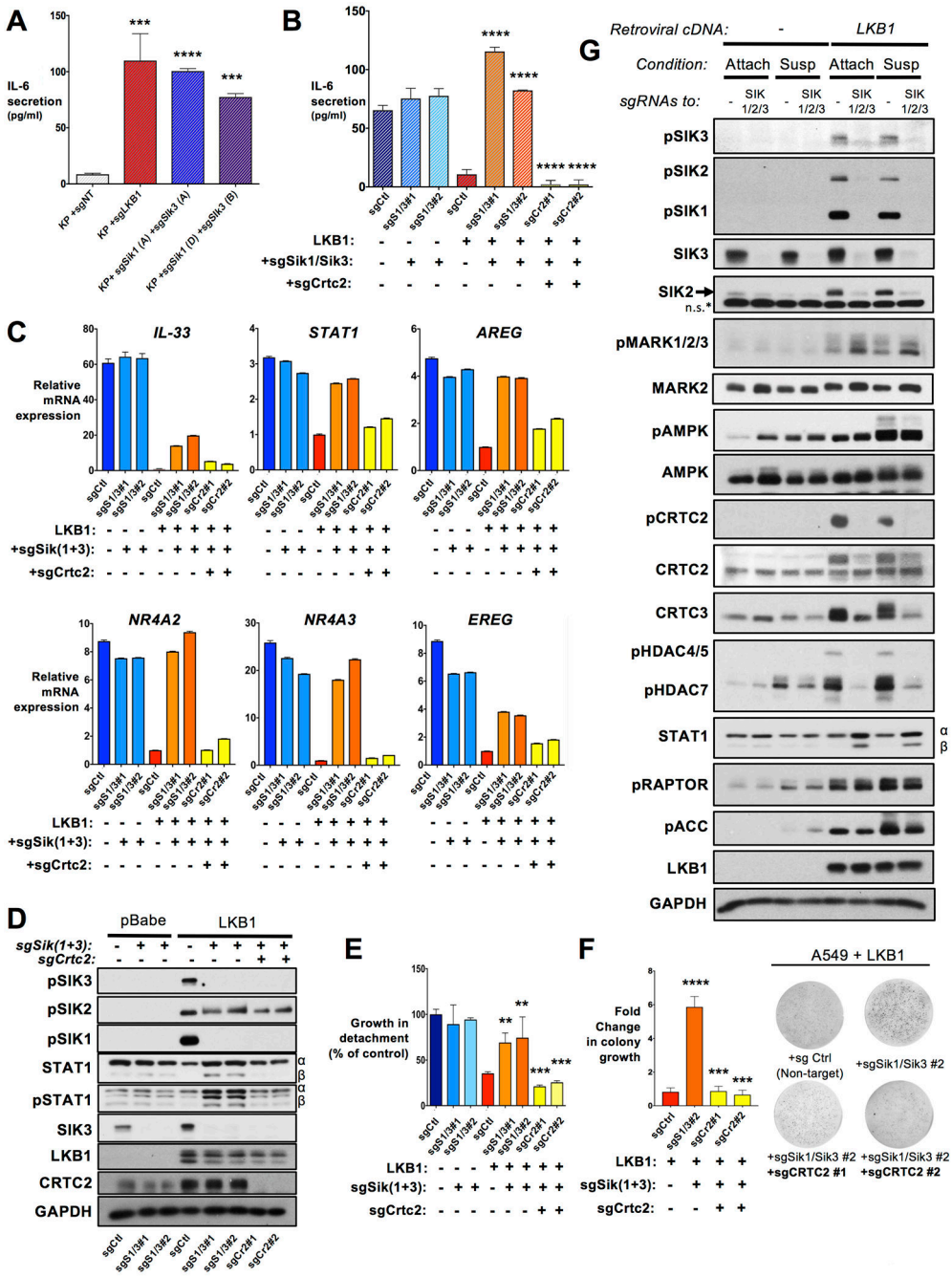

Figure 5. Functional analysis of murine and human NSCLC cell lines bearing LKB1 or SIK kinase family inactivation reveals CRTC2 dependent-induction of cytokine signaling and control of cell proliferation and growth under anchorage-free conditions.

(A) ELISA analysis of IL-6 secretion in mouse KP lines. KP cells lines were transduced with a sgRNA guide targeting Lkb1 or with two independent sets of guides to target Sik1 and Sik3 simultaneously. 500,000 control or KO cells were seeded in 6 well plates and supernatant was collected at 48hrs to quantitate the amount of IL6 released by the cells into the media.

(B) ELISA analysis of IL-6 secretion in human A549 NSCLC cells. Two independent cell lines bearing distinct guides to simultaneously target Sik1 and Sik3 were generated each in pBabe cells (LKB1-null) and in cells reconstituted with Lkb1 cDNA. Additionally, the LKB1-reconstituted sgSik1/3 cell line #2 was further targeted with one of two guides to target expression of Crtc2 or a control guide. 500,000 cells from each genotype were seeded and supernant was collected at 48 hrs and IL6 secretion was quantitated by ELISA.
(C) Relative expression of genes commonly regulated by LKB1, SIK1+3 kinases and CRTC2. qPCR was performed on pBabe and LKB1-expressing A549s, ± sgSik1+3 and ± sgCrtc2 guides to assess modulation of SIK1+3 and CRTC2-dependent transcription. For all genes examined, mRNA expression was plotted relative to LKB1-expressing control line (A549 LKB1 + sgCtI).
(D) Immunoblots from sgSIK1+3 A549 (Control or Lkb1-reconstituted) and sgSIK1+3+sgCrtc2 cell lines were assessed for expression and phosphorylation status of SIK kinases
(E) Proliferation of cells under anoikis (attachment-free) conditions. Control pBabe or Lkb1-expressing A549 cells expressing guides targeting Sik1 + Sik3 +/− sgCrtc2 guides were challenged with detachment conditions for 5 days. The number of surviving cells was quantitated with cyquant staining. Data are means of triplicate wells ± s.d.
(F) Left: Fold change in colony growth in soft agar of LKB1-expressing A549 cells expressing guides targeting Sik1 + Sik3 +/− sgCrtc2 guides. Colonies were counted at four weeks and the data are shown as the average of two biological replicates of triplicate wells for each genotype ± s.e.m. Right: representative images of colony formation in soft agar at experimental endpoint.
(G) Western immunoblots of lysates from Lkb1-null pBabe or Lkb1-expressing A549s, further expressing sgRNA guides targeting all three SIK kinases. Lysates were collected from cells under adherent and suspension conditions. Immunoblots depict phosphorylation status of the SIKs and additional AMPKRs (AMPK, MARKs), direct SIK kinase substrates (CRTCs, HDACs) and AMPKR targets or downstream transcriptionally regulated genes.